POLITECNICO DI TORINO
Repository ISTITUZIONALE

Observations of the Cabibbo-Suppressed decays $_{c}^{+}\to n^{+}^{0}$, $n^{+}^{-}^{+}$ and the Cabibbo-Favored decay

Original
Observations of the Cabibbo-Suppressed decays $_{c}^{+}\to n^{+}^{0}$, $n^{+}^{-}^{+}$ and the Cabibbo-Favored decay $_{c}^{+}\to nK^{-}^{+}^{+}$ / Collaboration, B., Ablikim, M., Achasov, M.N., Adlarson, P., Albrecht, M., Aliberti, R., Amoroso, A., An, M.R., An, Q., Bai, Y., Bakina, O., Baldini Ferroli, R., Balossino, I., Ban, Y., Batozskaya, V., Becker, D., Begzsuren, K., Berger, N., Bertani, M., Bettoni, D., et al.. - In: CHINESE PHYSICS C. - ISSN 1674-1137. - ELETTRONICO. - 47:2(2023), pp. 1-18. [10.1088/1674-1137/ac9d29]

Availability:
This version is available at: 11583/2973849 since: 2023-01-30T20:51:24Z

Publisher:
IOP Publishing Ltd

Published
DOI:10.1088/1674-1137/ac9d29

Terms of use:

This article is made available under terms and conditions as specified in the corresponding bibliographic description in the repository

Publisher copyright

(Article begins on next page)

02 November 2026

PAPER • OPEN ACCESS

Observations of the Cabibbo-Suppressed decays $\Lambda_c^+ \to n\pi^+\pi^0$, $n\pi^+\pi^-\pi^+$ and the Cabibbo-Favored decay $\Lambda_c^+ \to nK^-\pi^+\pi^+$

To cite this article: M. Ablikim *et al* 2023 *Chinese Phys. C* **47** 023001

View the article online for updates and enhancements.

You may also like

- Properties and Astrophysical Implications of the 150 *M* Binary Black Hole Merger GW190521
R. Abbott, T. D. Abbott, S. Abraham et al.
- First Measurement of the Hubble Constant from a Dark Standard Siren using the Dark Energy Survey Galaxies and the LIGO/Virgo Binary–Black-hole Merger GW170814
M. Soares-Santos, A. Palmese, W. Hartley et al.
- Overview of the JET results in support to ITER
X. Litaudon, S. Abduallev, M. Abhangi et al.

This content was downloaded from IP address 212.31.240.234 on 24/01/2023 at 11:31

Editors' Suggestion

Observations of the Cabibbo-Suppressed decays $\Lambda_c^+ \to n\pi^+\pi^0$, $n\pi^+\pi^-\pi^+$ and the Cabibbo-Favored decay $\Lambda_c^+ \to nK^-\pi^+\pi^+$*

M. Ablikim(麦迪娜)[1] M. N. Achasov[11,b] P. Adlarson[70] M. Albrecht[4] R. Aliberti[31] A. Amoroso[69A,69C] M. R. An(安美儒)[35] Q. An(安琪)[53,66] Y. Bai(白羽)[52] O. Bakina[32] R. Baldini Ferroli[26A] I. Balossino[27A,1] Y. Ban(班勇)[42,g] V. Batozskaya[1,40] D. Becker[31] K. Begzsuren[29] N. Berger[31] M. Bertani[26A] D. Bettoni[27A] F. Bianchi[69A,69C] E. Bianco[69A,69C] J. Bloms[63] A. Bortone[69A,69C] I. Boyko[32] R. A. Briere[5] A. Brueggemann[63] H. Cai(蔡浩)[71] X. Cai(蔡啸)[1,53] A. Calcaterra[26A] G. F. Cao(曹国富)[1,58] N. Cao(曹宁)[1,58] S. A. Cetin[57A] J. F. Chang(常劲帆)[1,53] W. L. Chang(常万玲)[1,58] G. R. Che(车国荣)[39] G. Chelkov[32,a] C. Chen(陈琛)[39] Chao Chen(陈超)[50] G. Chen(陈刚)[1] H. S. Chen(陈和生)[1,58] M. L. Chen(陈玛丽)[1,53] S. J. Chen(陈申见)[38] S. M. Chen(陈少敏)[56] T. Chen[1] X. R. Chen(陈旭荣)[28,58] X. T. Chen[1] Y. B. Chen(陈元柏)[1,53] Z. J. Chen(陈卓俊)[23,h] W. S. Cheng(成伟帅)[69C] S. K. Choi[50] X. Chu(初晓)[39] G. Cibinetto[27A] F. Cossio[69C] J. J. Cui(崔佳佳)[45] H. L. Dai(代洪亮)[1,53] J. P. Dai(代建平)[73] A. Dbeyssi[17] R. E. de Boer[4] D. Dedovich[32] Z. Y. Deng(邓子艳)[1] A. Denig[31] I. Denysenko[32] M. Destefanis[69A,69C] F. De Mori[69A,69C] Y. Ding(丁勇)[36] Y. Ding(丁逸)[30] J. Dong(董静)[1,53] L. Y. Dong(董燎原)[1,58] M. Y. Dong(董明义)[1] X. Dong(董翔)[71] S. X. Du(杜书先)[75] Z. H. Duan(段宗欢)[38] P. Egorov[32,a] Y. L. Fan(范玉兰)[71] J. Fang(方建)[1,53] S. S. Fang(房双世)[1,58] W. X. Fang(方文兴)[1] Y. Fang(方易)[1] R. Farinelli[27A] L. Fava[69B,69C] F. Feldbauer[4] G. Felici[26A] C. Q. Feng(封常青)[53,66] J. H. Feng(冯俊华)[54] K Fischer[64] M. Fritsch[4] C. Fritzsch[63] C. D. Fu(傅成栋)[1] H. Gao(高涵)[58] Y. N. Gao(高原宁)[42,g] Yang Gao(高扬)[53,66] S. Garbolino[69C] I. Garzia[27A,27B] P. T. Ge(葛潘婷)[71] Z. W. Ge(葛振武)[38] C. Geng(耿聪)[54] E. M. Gersabeck[62] A Gilman[64] K. Goetzen[12] L. Gong(龚丽)[36] W. X. Gong(龚文煊)[1,53] W. Gradl[31] M. Greco[69A,69C] L. M. Gu(谷立民)[38] M. H. Gu(顾旻皓)[1,53] Y. T. Gu(顾运厅)[14] C. Y Guan(关春懿)[1,58] A. Q. Guo(郭爱强)[28,58] L. B. Guo(郭立波)[37] R. P. Guo(郭如盼)[44] Y. P. Guo(郭玉萍)[10,f] A. Guskov[32,a] W. Y. Han(韩文颖)[35] X. Q. Hao(郝喜庆)[18] F. A. Harris[60] K. K. He(何凯凯)[50] K. L. He(何康林)[1,58] F. H. Heinsius[4] C. H. Heinz[31] Y. K. Heng(衡月昆)[1] C. Herold[55] G. Y. Hou(侯国一)[1,58] Y. R. Hou(侯颖锐)[58] Z. L. Hou(侯治龙)[1] H. M. Hu(胡海明)[1,58] J. F. Hu[51,i] T. Hu(胡涛)[1] Y. Hu(胡誉)[1] G. S. Huang(黄光顺)[53,66] K. X. Huang(黄凯旋)[54] L. Q. Huang(黄麟钦)[28,58] X. T. Huang(黄性涛)[45] Y. P. Huang(黄燕萍)[1] Z. Huang(黄震)[42,g] T. Hussain[68] N Hüsken[25,31] W. Imoehl[25] M. Irshad[53,66] J. Jackson[25] S. Jaeger[4] S. Janchiv[29] E. Jang[50] J. H. Jeong[50] Q. Ji(纪全)[1] Q. P. Ji(姬清平)[18] X. B. Ji(季晓斌)[1,58] X. L. Ji(季筱璐)[1,53] Y. Y. Ji(吉钰瑶)[45] Z. K. Jia(贾泽坤)[53,66] S. S. Jiang(姜赛赛)[35] X. S. Jiang(江晓山)[1] Y. Jiang[58] J. B. Jiao(焦健斌)[45] Z. Jiao(焦铮)[21] S. Jin(金山)[38] Y. Jin(金毅)[61]

Received 10 October 2022; Accepted 26 October 2022; Published online 31 October 2022

* Supported in part by National Key R & D Program of China (2020YFA0406400, 2020YFA0406300); National Natural Science Foundation of China (NSFC) (11635010, 11735014, 11805086, 11835012, 11935015, 11935016, 11935018, 11975011, 11961141012, 12022510, 12025502, 12035009, 12035013, 12192260, 12192261, 12192262, 12192263, 12192264, 12192265); the Chinese Academy of Sciences (CAS) Large-Scale Scientific Facility Program; Joint Large-Scale Scientific Facility Funds of the NSFC and CAS (U1832207); the CAS Center for Excellence in Particle Physics (CCEPP); 100 Talents Program of CAS; Fundamental Research Funds for the Central Universities, Lanzhou University, University of Chinese Academy of Sciences; The Institute of Nuclear and Particle Physics (INPAC) and Shanghai Key Laboratory for Particle Physics and Cosmology; ERC (758462); German Research Foundation DFG (443159800), Collaborative Research Center CRC 1044, GRK 2149; Istituto Nazionale di Fisica Nucleare, Italy; Ministry of Development of Turkey (DPT2006K-120470); National Science and Technology fund; National Science Research and Innovation Fund (NSRF) via the Program Management Unit for Human Resources & Institutional Development, Research and Innovation (B16F640076; STFC) (United Kingdom); Suranaree University of Technology (SUT), Thailand Science Research and Innovation (TSRI), and National Science Research and Innovation Fund (NSRF) (160355); The Royal Society, UK (DH140054, DH160214); The Swedish Research Council; U. S. Department of Energy (DE-FG02-05ER41374)

Content from this work may be used under the terms of the Creative Commons Attribution 3.0 licence. Any further distribution of this work must maintain attribution to the author(s) and the title of the work, journal citation and DOI. Article funded by SCOAP[3] and published under licence by Chinese Physical Society and the Institute of High Energy Physics of the Chinese Academy of Sciences and the Institute of Modern Physics of the Chinese Academy of Sciences and IOP Publishing Ltd

M. Q. Jing(荆茂强)[1,58] T. Johansson[70] N. Kalantar-Nayestanaki[59] X. S. Kang(康晓珅)[36] R. Kappert[59] M. Kavatsyuk[59] B. C. Ke(柯百谦)[75] I. K. Keshk[4] A. Khoukaz[63] R. Kiuchi[1] R. Kliemt[12] L. Koch[33] O. B. Kolcu[57A] B. Kopf[4] M. Kuemmel[4] M. Kuessner[4] A. Kupsc[40,70] W. Kühn[33] J. J. Lane[62] J. S. Lange[33] P. Larin[17] A. Lavania[24] L. Lavezzi[69A,69C] Z. H. Lei(雷祚弘)[53,66] H. Leithoff[31] M. Lellmann[31] T. Lenz[31] C. Li(李翠)[43] C. Li(李聪)[39] C. H. Li(李春花)[35] Cheng Li(李澄)[53,66] D. M. Li(李德民)[75] F. Li(李飞)[1,53] G. Li(李刚)[1] H. Li(李慧)[47] H. Li(李贺)[53,66] H. B. Li(李海波)[1,58] H. J. Li(李惠静)[18] H. N. Li[51,i] J. Q. Li[4] J. S. Li(李静舒)[54] J. W. Li(李井文)[45] Ke Li(李科)[1] L. J Li[1] L. K. Li(李龙科)[1] Lei Li(李蕾)[3] M. H. Li(李明浩)[39] P. R. Li(李培荣)[34,j,k] S. X. Li(李素娴)[10] S. Y. Li(栗帅迎)[56] T. Li(李腾)[45] W. D. Li(李卫东)[1,58] W. G. Li(李卫国)[1] X. H. Li(李旭红)[53,66] X. L. Li(李晓玲)[45] Xiaoyu Li(李晓宇)[1,58] Y. G. Li(李彦谷)[42,g] Z. X. Li(李振轩)[14] Z. Y. Li(李紫源)[54] C. Liang(梁畅)[38] H. Liang(梁昊)[53,66] H. Liang(梁浩)[1,58] H. Liang(梁浩)[30] Y. F. Liang(梁勇飞)[49] Y. T. Liang(梁羽铁)[28,58] G. R. Liao(廖广睿)[13] L. Z. Liao(廖龙洲)[45] J. Libby[24] A. Limphirat[55] C. X. Lin(林创新)[54] D. X. Lin(林德旭)[28,58] T. Lin[1] B. J. Liu(刘北江)[1] C. Liu(刘成)[30] C. X. Liu(刘春秀)[1] D. Liu[17,66] F. H. Liu(刘福虎)[48] Fang Liu(刘芳)[1] Feng Liu(刘峰)[6] G. M. Liu[51,i] H. Liu[34,j,k] H. B. Liu(刘宏邦)[14] H. M. Liu(刘怀民)[1,58] Huanhuan Liu(刘欢欢)[1] Huihui Liu(刘汇慧)[19] J. B. Liu(刘建北)[53,66] J. L. Liu(刘佳俊)[67] J. Y. Liu(刘晶译)[1,58] K. Liu(刘凯)[1] K. Y. Liu(刘魁勇)[36] Ke Liu(刘珂)[20] L. Liu(刘亮)[53,66] Lu Liu(刘露)[39] M. H. Liu(刘美宏)[10,f] P. L. Liu(刘佩莲)[1] Q. Liu(刘倩)[58] S. B. Liu(刘树彬)[53,66] T. Liu(刘桐)[10,f] W. K. Liu(刘维克)[39] W. M. Liu(刘卫民)[53,66] X. Liu(刘翔)[34,j,k] Y. Liu(刘英)[34,j,k] Y. B. Liu(刘玉斌)[39] Z. A. Liu(刘振安)[1] Z. Q. Liu(刘智青)[45] X. C. Lou(娄辛丑)[1] F. X. Lu(卢飞翔)[54] H. J. Lu(吕海江)[21] J. G. Lu(吕军光)[1,53] X. L. Lu(陆小玲)[1] Y. Lu(卢宇)[7] Y. P. Lu(卢云鹏)[1,53] Z. H. Lu[1] C. L. Luo(罗成林)[37] M. X. Luo(罗民兴)[74] T. Luo(罗涛)[10,f] X. L. Luo(罗小兰)[1,53] X. R. Lyu(吕晓睿)[58] Y. F. Lyu(吕翌丰)[39] F. C. Ma(马凤才)[36] H. L. Ma(马海龙)[1] L. L. Ma(马连良)[45] M. M. Ma(马明明)[1,58] Q. M. Ma(马秋梅)[1] R. Q. Ma(马润秋)[1,58] R. T. Ma(马瑞廷)[58] X. Y. Ma(马骁妍)[1,53] Y. Ma(马尧)[42,g] F. E. Maas[17] M. Maggiora[69A,69C] S. Maldaner[4] S. Malde[64] Q. A. Malik[68] A. Mangoni[26B] Y. J. Mao(冒亚军)[42,g] Z. P. Mao(毛泽普)[1] S. Marcello[69A,69C] Z. X. Meng(孟召霞)[61] J. G. Messchendorp[12,59] G. Mezzadri[27A,1] H. Miao[1] T. J. Min(闵天觉)[38] R. E. Mitchell[25] X. H. Mo(莫晓虎)[1] N. Yu. Muchnoi[11,b] Y. Nefedov[32] F. Nerling[17,d] I. B. Nikolaev[11,b] Z. Ning(宁哲)[1,53] S. Nisar[9,l] Y. Niu(牛艳)[45] S. L. Olsen[58] Q. Ouyang(欧阳群)[1] S. Pacetti[26B,26C] X. Pan(潘祥)[10,f] Y. Pan(潘越)[52] A. Pathak[30] P. Patteri[26A] M. Pelizaeus[4] H. P. Peng(彭海平)[53,66] K. Peters[12,d] J. L. Ping(平加伦)[37] R. G. Ping(平荣刚)[1,58] S. Plura[31] S. Pogodin[32] V. Prasad[53,66] F. Z. Qi(齐法制)[1] H. Qi(齐航)[53,66] H. R. Qi(漆红荣)[56] M. Qi(祁鸣)[38] T. Y. Qi(齐天钰)[10,f] S. Qian(钱森)[1,53] W. B. Qian(钱文斌)[58] Z. Qian(钱圳)[54] C. F. Qiao(乔从丰)[58] J. J. Qin(秦佳佳)[67] L. Q. Qin(秦丽清)[13] X. P. Qin(覃潇平)[10,f] X. S. Qin(秦小帅)[45] Z. H. Qin(秦中华)[1,53] J. F. Qiu(邱进发)[1] S. Q. Qu(屈三强)[56] K. H. Rashid[68] C. F. Redmer[31] K. J. Ren(任旷洁)[35] A. Rivetti[69C] V. Rodin[59] M. Rolo[69C] G. Rong(荣刚)[1,58] Ch. Rosner[17] S. N. Ruan(阮氏宁)[39] A. Sarantsev[32,c] Y. Schelhaas[31] C. Schnier[4] K. Schoenning[70] M. Scodeggio[27A,27B] K. Y. Shan(尚科羽)[10,f] W. Shan(单葳)[22] X. Y. Shan(单心钰)[53,66] J. F. Shangguan(上官剑锋)[50] L. G. Shao(邵立港)[1,58] M. Shao(邵明)[53,66] C. P. Shen(沈成平)[10,f] H. F. Shen(沈宏飞)[1,58] X. Y. Shen(沈肖雁)[1,58] B. A. Shi(施伯安)[58] H. C. Shi(石煌超)[53,66] J. Y. Shi(石京燕)[1] Q. Q. Shi(石勤强)[50] R. S. Shi(师荣盛)[1,58] X. Shi(史欣)[1,53] X. D. Shi(师晓东)[53,66] J. J. Song(宋娇娇)[18] W. M. Song(宋维民)[1,30] Y. X. Song(宋昀轩)[42,g] S. Sosio[69A,69C] S. Spataro[69A,69C] F. Stieler[31] K. X. Su(苏可馨)[71] P. P. Su(苏彭彭)[50] Y. J. Su(粟杨捷)[58] G. X. Sun(孙功星)[1] H. Sun[58] H. K. Sun(孙浩凯)[1] J. F. Sun(孙俊峰)[18] L. Sun(孙亮)[71] S. S. Sun(孙胜森)[1,58] T. Sun(孙童)[1,58] W. Y. Sun(孙文玉)[30] Y. J. Sun(孙勇杰)[53,66] Y. Z. Sun(孙永昭)[1] Z. T. Sun(孙振田)[45] Y. H. Tan(谭英华)[71] Y. X. Tan(谭雅星)[53,66] C. J. Tang(唐昌建)[49] G. Y. Tang(唐光毅)[1] J. Tang(唐健)[54] L. Y Tao(陶璐燕)[67] Q. T. Tao(陶秋田)[23,h] M. Tat[64] J. X. Teng(滕佳秀)[53,66] V. Thoren[70] W. H. Tian(田文辉)[47] Y. Tian(田野)[28,58] I. Uman[57B] B. Wang(王斌)[1] B. L. Wang(王滨龙)[58] C. W. Wang(王成伟)[38] D. Y. Wang(王大勇)[42,g] F. Wang(王菲)[67] H. J. Wang(王泓鉴)[34,j,k] H. P. Wang(王宏鹏)[1,58] K. Wang(王科)[1,53] L. L. Wang(王亮亮)[1] M. Wang(王萌)[45] M. Z. Wang(王梦真)[42,g] Meng Wang(王蒙)[1,58] S. Wang[13] S. Wang(王顺)[10,f] T. Wang(王婷)[10,f] T. J. Wang(王腾蛟)[39] W. Wang(王为)[54]

W. H. Wang(王文欢)[71] W. P. Wang(王维平)[53,66] X. Wang(王轩)[42,g] X. F. Wang(王雄飞)[34,j,k]
X. L. Wang(王小龙)[10,f] Y. Wang(王亦)[56] Y. D. Wang(王雅迪)[41] Y. F. Wang(王贻芳)[1] Y. H. Wang(王英豪)[43]
Y. Q. Wang(王雨晴)[1] Yaqian Wang(王亚乾)[1,16] Z. Wang(王铮)[1,53] Z. Y. Wang(王至勇)[1,58] Ziyi Wang(王子一)[58]
D. H. Wei(魏代会)[13] F. Weidner[63] S. P. Wen(文硕频)[1] D. J. White[62] U. Wiedner[4] G. Wilkinson[64]
M. Wolke[70] L. Wollenberg[4] J. F. Wu(吴金飞)[1,58] L. H. Wu(伍灵慧)[1] L. J. Wu(吴连近)[1,58] X. Wu(吴潇)[10,f]
X. H. Wu(伍雄浩)[30] Y. Wu[66] Y. J Wu(吴英杰)[28] Z. Wu(吴智)[1,53] L. Xia(夏磊)[53,66] T. Xiang(相腾)[42,g]
D. Xiao(肖栋)[34,j,k] G. Y. Xiao(肖光延)[38] H. Xiao(肖浩)[10,f] S. Y. Xiao(肖素玉)[1] Y. L. Xiao(肖云龙)[10,f]
Z. J. Xiao(肖振军)[37] C. Xie(谢陈)[38] X. H. Xie(谢昕海)[42,g] Y. Xie(谢勇)[45] Y. G. Xie(谢宇广)[1,53]
Y. H. Xie(谢跃红)[6] Z. P. Xie(谢智鹏)[53,66] T. Y. Xing(邢天宇)[1,58] C. F. Xu[1] C. J. Xu(许创杰)[54]
G. F. Xu(许国发)[1] H. Y. Xu(许皓月)[61] Q. J. Xu(徐庆君)[15] X. P. Xu(徐新平)[50] Y. C. Xu(胥英超)[58]
Z. P. Xu(许泽鹏)[38] F. Yan(严芳)[10,f] L. Yan(严亮)[10,f] W. B. Yan(鄢文标)[53,66] W. C. Yan(闫文成)[75]
H. J. Yang(杨海军)[46,e] H. L. Yang(杨昊霖)[30] H. X. Yang(杨洪勋)[1] L. Yang(杨玲)[47] Tao Yang(杨涛)[1]
Y. F. Yang(杨艳芳)[39] Y. X. Yang(杨逸翔)[1,58] Yifan Yang(杨翊凡)[1,58] M. Ye(叶梅)[1,53] M. H. Ye(叶铭汉)[8]
J. H. Yin(殷俊昊)[1] Z. Y. You(尤郑昀)[54] B. X. Yu(俞伯祥)[1] C. X. Yu(喻纯旭)[39] G. Yu(余刚)[1,58] T. Yu(于涛)[67]
X. D. Yu(余旭东)[42,g] C. Z. Yuan(苑长征)[1,58] L. Yuan(袁丽)[2] S. C. Yuan[1] X. Q. Yuan(袁晓庆)[1]
Y. Yuan(袁野)[1,58] Z. Y. Yuan(袁朝阳)[54] C. X. Yue(岳崇兴)[35] A. A. Zafar[68] F. R. Zeng(曾凡蕊)[45]
X. Zeng(曾鑫)[6] Y. Zeng(曾云)[23,h] X. Y. Zhai(翟星晔)[30] Y. H. Zhan(詹永华)[54] A. Q. Zhang(张安庆)[1]
B. L. Zhang[1] B. X. Zhang(张丙新)[1] D. H. Zhang(张丹昊)[39] G. Y. Zhang(张广义)[18] H. Zhang[66]
H. H. Zhang(张宏浩)[54] H. H. Zhang(张宏宏)[30] H. Y. Zhang(章红宇)[1,53] J. L. Zhang(张杰磊)[72]
J. Q. Zhang(张敬庆)[37] J. W. Zhang(张家文)[1] J. X. Zhang[34,j,k] J. Y. Zhang(张建勇)[1] J. Z. Zhang(张景芝)[1,58]
Jianyu Zhang(张剑宇)[1,58] Jiawei Zhang(张嘉伟)[1,58] L. M. Zhang(张黎明)[56] L. Q. Zhang(张丽青)[54]
Lei Zhang(张雷)[38] P. Zhang[1] Q. Y. Zhang(张秋岩)[35,75] Shuihan Zhang(张水涵)[1,58] Shulei Zhang(张书磊)[23,h]
X. D. Zhang(张小东)[41] X. M. Zhang[1] X. Y. Zhang(张学尧)[45] X. Y. Zhang(张旭颜)[50] Y. Zhang[64]
Y. T. Zhang(张亚腾)[75] Y. H. Zhang(张银鸿)[1,53] Yan Zhang(张言)[53,66] Yao Zhang(张瑶)[1] Z. H. Zhang[1]
Z. L. Zhang(张兆领)[30] Z. Y. Zhang(张振宇)[71] Z. Y. Zhang(张子羽)[39] G. Zhao(赵光)[1] J. Zhao(赵静)[35]
J. Y. Zhao(赵静宜)[1,58] J. Z. Zhao(赵京周)[1,53] Lei Zhao(赵雷)[53,66] Ling Zhao(赵玲)[1] M. G. Zhao(赵明刚)[39]
S. J. Zhao(赵书俊)[75] Y. B. Zhao(赵豫斌)[1,53] Y. X. Zhao(赵宇翔)[28,58] Z. G. Zhao(赵政国)[53,66] A. Zhemchugov[32,a]
B. Zheng(郑波)[67] J. P. Zheng(郑建平)[1,53] Y. H. Zheng(郑阳恒)[58] B. Zhong(钟彬)[37] C. Zhong(钟翠)[67]
X. Zhong(钟鑫)[54] H. Zhou(周航)[45] L. P. Zhou(周利鹏)[1,58] X. Zhou(周详)[71] X. K. Zhou(周晓康)[58]
X. R. Zhou(周小蓉)[53,66] X. Y. Zhou(周兴玉)[35] Y. Z. Zhou(周祎卓)[10,f] J. Zhu(朱江)[39] K. Zhu(朱凯)[1]
K. J. Zhu(朱科军)[1] L. X. Zhu(朱琳萱)[58] S. H. Zhu(朱世海)[65] S. Q. Zhu(朱仕强)[38] T. J. Zhu(朱腾蛟)[72]
W. J. Zhu(朱文静)[10,f] Y. C. Zhu(朱莹春)[53,66] Z. A. Zhu(朱自安)[1,58] J. H. Zou(邹佳恒)[1]

(BESIII Collaboration)

[1]Institute of High Energy Physics, Beijing 100049, China
[2]Beihang University, Beijing 100191, China
[3]Beijing Institute of Petrochemical Technology, Beijing 102617, China
[4]Bochum Ruhr-University, D-44780 Bochum, Germany
[5]Carnegie Mellon University, Pittsburgh, Pennsylvania 15213, USA
[6]Central China Normal University, Wuhan 430079, China
[7]Central South University, Changsha 410083, China
[8]China Center of Advanced Science and Technology, Beijing 100190, China
[9]COMSATS University Islamabad, Lahore Campus, Defence Road, Off Raiwind Road, 54000 Lahore, Pakistan
[10]Fudan University, Shanghai 200433, China
[11]G.I. Budker Institute of Nuclear Physics SB RAS (BINP), Novosibirsk 630090, Russia
[12]GSI Helmholtzcentre for Heavy Ion Research GmbH, D-64291 Darmstadt, Germany
[13]Guangxi Normal University, Guilin 541004, China
[14]Guangxi University, Nanning 530004, China
[15]Hangzhou Normal University, Hangzhou 310036, China
[16]Hebei University, Baoding 071002, China
[17]Helmholtz Institute Mainz, Staudinger Weg 18, D-55099 Mainz, Germany
[18]Henan Normal University, Xinxiang 453007, China
[19]Henan University of Science and Technology, Luoyang 471003, China

[20]Henan University of Technology, Zhengzhou 450001, China
[21]Huangshan College, Huangshan 245000, China
[22]Hunan Normal University, Changsha 410081, China
[23]Hunan University, Changsha 410082, China
[24]Indian Institute of Technology Madras, Chennai 600036, India
[25]Indiana University, Bloomington, Indiana 47405, USA
[26A]INFN Laboratori Nazionali di Frascati, I-00044, Frascati, Italy
[26B]INFN Sezione di Perugia, I-06100, Perugia, Italy
[26C]University of Perugia, I-06100, Perugia, Italy
[27A]INFN Sezione di Ferrara, I-44122, Ferrara, Italy
[27B]University of Ferrara, I-44122, Ferrara, Italy
[28]Institute of Modern Physics, Lanzhou 730000, China
[29]Institute of Physics and Technology, Peace Avenue 54B, Ulaanbaatar 13330, Mongolia
[30]Jilin University, Changchun 130012, China
[31]Johannes Gutenberg University of Mainz, Johann-Joachim-Becher-Weg 45, D-55099 Mainz, Germany
[32]Joint Institute for Nuclear Research, 141980 Dubna, Moscow region, Russia
[33]Justus-Liebig-Universitaet Giessen, II. Physikalisches Institut, Heinrich-Buff-Ring 16, D-35392 Giessen, Germany
[34]Lanzhou University, Lanzhou 730000, China
[35]Liaoning Normal University, Dalian 116029, China
[36]Liaoning University, Shenyang 110036, China
[37]Nanjing Normal University, Nanjing 210023, China
[38]Nanjing University, Nanjing 210093, China
[39]Nankai University, Tianjin 300071, China
[40]National Centre for Nuclear Research, Warsaw 02-093, Poland
[41]North China Electric Power University, Beijing 102206, China
[42]Peking University, Beijing 100871, China
[43]Qufu Normal University, Qufu 273165, China
[44]Shandong Normal University, Jinan 250014, China
[45]Shandong University, Jinan 250100, China
[46]Shanghai Jiao Tong University, Shanghai 200240, China
[47]Shanxi Normal University, Linfen 041004, China
[48]Shanxi University, Taiyuan 030006, China
[49]Sichuan University, Chengdu 610064, China
[50]Soochow University, Suzhou 215006, China
[51]South China Normal University, Guangzhou 510006, China
[52]Southeast University, Nanjing 211100, China
[53]State Key Laboratory of Particle Detection and Electronics, Beijing 100049, Hefei 230026, China
[54]Sun Yat-Sen University, Guangzhou 510275, China
[55]Suranaree University of Technology, University Avenue 111, Nakhon Ratchasima 30000, Thailand
[56]Tsinghua University, Beijing 100084, China
[57A]Istinye University, 34010, Istanbul, Turkey
[57B]Near East University, Nicosia, North Cyprus, Mersin 10, Turkey
[58]University of Chinese Academy of Sciences, Beijing 100049, China
[59]University of Groningen, NL-9747 AA Groningen, The Netherlands
[60]University of Hawaii, Honolulu, Hawaii 96822, USA
[61]University of Jinan, Jinan 250022, China
[62]University of Manchester, Oxford Road, Manchester, M13 9PL, United Kingdom
[63]University of Muenster, Wilhelm-Klemm-Strasse 9, 48149 Muenster, Germany
[64]University of Oxford, Keble Road, Oxford OX13RH, United Kingdom
[65]University of Science and Technology Liaoning, Anshan 114051, China
[66]University of Science and Technology of China, Hefei 230026, China
[67]University of South China, Hengyang 421001, China
[68]University of the Punjab, Lahore-54590, Pakistan
[69A]University of Turin, I-10125, Turin, Italy
[69B]University of Eastern Piedmont, I-15121, Alessandria, Italy
[69C]INFN, I-10125, Turin, Italy
[70]Uppsala University, Box 516, SE-75120 Uppsala, Sweden
[71]Wuhan University, Wuhan 430072, China
[72]Xinyang Normal University, Xinyang 464000, China
[73]Yunnan University, Kunming 650500, China
[74]Zhejiang University, Hangzhou 310027, China
[75]Zhengzhou University, Zhengzhou 450001, China
[a]Also at the Moscow Institute of Physics and Technology, Moscow 141700, Russia
[b]Also at the Novosibirsk State University, Novosibirsk, 630090, Russia
[c]Also at the NRC "Kurchatov Institute", PNPI, 188300, Gatchina, Russia
[d]Also at Goethe University Frankfurt, 60323 Frankfurt am Main, Germany
[e]Also at Key Laboratory for Particle Physics, Astrophysics and Cosmology, Ministry of Education; Shanghai Key Laboratory for Particle Physics and Cosmology; Institute of Nuclear and Particle Physics, Shanghai 200240, China

[f]Also at Key Laboratory of Nuclear Physics and Ion-beam Application (MOE) and Institute of Modern Physics, Fudan University, Shanghai 200443, China
[g]Also at State Key Laboratory of Nuclear Physics and Technology, Peking University, Beijing 100871, China
[h]Also at School of Physics and Electronics, Hunan University, Changsha 410082, China
[i]Also at Guangdong Provincial Key Laboratory of Nuclear Science, Institute of Quantum Matter, South China Normal University, Guangzhou 510006, China
[j]Also at Frontiers Science Center for Rare Isotopes, Lanzhou University, Lanzhou 730000, China
[k]Also at Lanzhou Center for Theoretical Physics, Lanzhou University, Lanzhou 730000, China
[l]Also at the Department of Mathematical Sciences, IBA, Karachi, Pakistan

Abstract: Using electron-positron annihilation data samples corresponding to an integrated luminosity of 4.5 fb^{-1}, collected by the BESIII detector in the energy region between 4599.53 MeV and 4698.82 MeV, we report the first observations of the Cabibbo-suppressed decays $\Lambda_c^+ \to n\pi^+\pi^0$, $\Lambda_c^+ \to n\pi^+\pi^-\pi^+$, and the Cabibbo-favored decay $\Lambda_c^+ \to nK^-\pi^+\pi^+$ with statistical significances of 7.9σ, 7.8σ, and $> 10\sigma$, respectively. The branching fractions of these decays are measured to be $\mathcal{B}(\Lambda_c^+ \to n\pi^+\pi^0) = (0.64 \pm 0.09 \pm 0.02)\%$, $\mathcal{B}(\Lambda_c^+ \to n\pi^+\pi^-\pi^+) = (0.45 \pm 0.07 \pm 0.03)\%$, and $\mathcal{B}(\Lambda_c^+ \to nK^-\pi^+\pi^+) = (1.90 \pm 0.08 \pm 0.09)\%$, where the first uncertainties are statistical and the second are systematic. We find that the branching fraction of the decay $\Lambda_c^+ \to n\pi^+\pi^0$ is about one order of magnitude higher than that of $\Lambda_c^+ \to n\pi^+$.

Keywords: Λ_c^+ baryon, Branching fraction, BESIII detector

DOI: 10.1088/1674-1137/ac9d29

I. INTRODUCTION

Charmed baryons provide an excellent laboratory for studying the properties of QCD in the case where a heavy quark couples to two light quarks. Currently, we do not have reliable phenomenological models to describe these complex baryon decays. More than two decades ago, a general formulation of a topological-diagram scheme for the nonleptonic weak decays of baryons was proposed to calculate the amplitudes of different topological diagrams [1]. The factorizable external W-emission amplitude T and internal W-emission amplitude C, as well as the non-factorizable inner W-emission amplitude C' and W-exchange amplitude E are introduced in the representation of these diagrams. In this scheme, one amplitude can be factorized into two parts, the decay constant of the emitted meson and the heavy-to-light transition form factor, which can be directly calculated. By way of example, the topological diagrams for $\Lambda_c^+ \to n\pi^+\pi^0$ can be seen in Fig. 1. We know that here the non-factorizable contribution is essential for understanding the weak decays of charmed baryons, in contrast to the negligible effect they contribute in heavy-meson decays [2]. Hence, studies of charmed baryon decays involving non-factorizable components are critical for understanding the underlying dynamics of charmed-baryon decays in general.

In addition, an alternative and model-inpendent approach based on quark flavor $SU(3)$ symmetry has been proposed to describe charmed-baryon decays. Even though it is an approximate method, it is a powerful and reliable tool to extract useful information about these transitions [3–10]. Improved measurements of charmed-baryon decays will be important in further testing the validity of this method.

Many experimental studies of various Λ_c^+ decays have been reported, with a focus on decays to two-body hadronic final states [11–21]. However, more studies of multi-body hadronic decays are required to gain deeper insight into the nature of non-perturbative QCD, as these involve rich intermediate processes and the branching fractions (BF) are in general higher. There is a significant discrepancy between the predicted BFs of $\Lambda_c^+ \to N\bar{K}\pi\pi$ decays reported in Ref. [22] and the measured values for $\Lambda_c^+ \to pK^-\pi^+\pi^0$ and $\Lambda_c^+ \to p\bar{K}^0\pi^+\pi^-$ [23]. Clarifying this tension requires knowledge of the BFs of hadronic Λ_c^+ decays to final states involving a neutron. Fewer studies have been performed for these decays because of the difficulty of direct neutron detection.

The BESIII collaboration has measured the BFs of the Cabibbo-favored (CF) decay $\Lambda_c^+ \to nK_S^0\pi^+$ [14] and the Cabibbo-suppressed (CS) decay $\Lambda_c^+ \to n\pi^+$ [18]. These studies provide critical tests for isospin and $SU(3)$ symmetries in charmed-baryon decays, the violation of which could lead to enhanced CP-violation effects [24, 25]. Taking the BFs of $\Lambda_c^+ \to nK_S^0\pi^+$, $\Lambda_c^+ \to pK_S^0\pi^0$ and $\Lambda_c^+ \to pK^-\pi^+$ from the Particle Data Group (PDG) [23], the amplitudes of these three decays satisfy the triangle relation and obey isospin symmetry [3]. However, the ratio of the BF of $\Lambda_c^+ \to n\pi^+$ to that of $\Lambda_c^+ \to p\pi^0$ is measured to be larger than 7.2 which disagrees with the $SU(3)$ flavor symmetry model prediction [3, 6, 26]. Precise measurements of the BFs of additional Λ_c^+ decays to final states involving a neutron, such as $\Lambda_c^+ \to n\pi^+\pi^0$, $\Lambda_c^+ \to n\pi^+\pi^-\pi^+$, and $\Lambda_c^+ \to nK^-\pi^+\pi^+$, are highly desirable to allow for futher tests of isospin and $SU(3)$ symmetries in charmed-baryon decays. Throughout this paper, charge-conjugate modes are implicitly assumed.

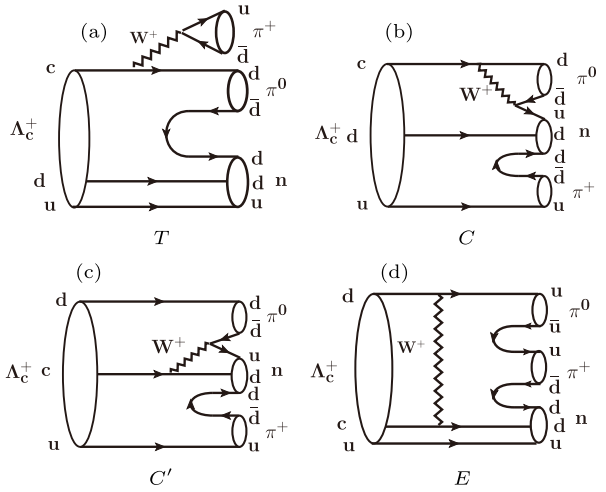


Fig. 1. Topological diagrams of the decay $\Lambda_c^+ \to n\pi^+\pi^0$ via (a) external W-emission T, (b) internal W-emission C, (c) inner W-emission C', and (d) W-exchange diagram E.

In this paper, two CS decays $\Lambda_c^+ \to n\pi^+\pi^0$, $\Lambda_c^+ \to n\pi^+\pi^-\pi^+$, and the CF decay $\Lambda_c^+ \to nK^-\pi^+\pi^+$ are studied by employing the double-tag (DT) method [27], where the neutron is reconstructed via the missing-mass technique. Our analysis is based on electron-positron annihilation data samples collected at seven center-of-mass (c.m.) energies from $\sqrt{s} = 4599.53$ MeV to 4698.82 MeV by the BESIII detector. These data samples correspond to an integrated luminosity of 4.5 fb^{-1} [28–31], as listed in Table 1. Within this energy range, the electron-positron collisions provide a clean environment for the production $\Lambda_c^+\bar{\Lambda}_c^-$ pairs, which offers a unique opportunity to carry out model-independent measurements of the BFs of various Λ_c^+ decays involving neutrons. The DT method allows us to measure the BFs without any theoretical input or external information on the cross section of Λ_c^+ production.

Table 1. The c.m. energies and integrated luminosities for the data samples.

$\sqrt{s}$ /MeV	Int. luminosity/pb^{-1}
4599.53	$586.90 \pm 0.10 \pm 3.90$
4611.86	$103.65 \pm 0.05 \pm 0.55$
4628.00	$521.53 \pm 0.11 \pm 2.76$
4640.91	$551.65 \pm 0.12 \pm 2.92$
4661.24	$529.43 \pm 0.12 \pm 2.81$
4681.92	$1667.39 \pm 0.21 \pm 8.84$
4698.82	$535.54 \pm 0.12 \pm 2.84$

The $\bar{\Lambda}_c^-$ baryons are reconstructed with twelve exclusive hadronic decay modes, as listed in Table 2. This data set is referred to as the single-tag (ST) sample. The π^0, K_S^0, $\bar{\Lambda}$, $\bar{\Sigma}^0$, and $\bar{\Sigma}^-$ particles are reconstructed via individual dominant decay modes. Those events in which any of the signal decays $\Lambda_c^+ \to n\pi^+\pi^0$, $\Lambda_c^+ \to n\pi^+\pi^-\pi^+$, and $\Lambda_c^+ \to nK^-\pi^+\pi^+$ are reconstructed in the system recoiling against the ST $\bar{\Lambda}_c^-$ candidates are denoted as DT candidates.

II. BESIII DETECTOR AND MONTE CARLO SIMULATION

The BESIII detector [32] records symmetric e^+e^- collisions provided by the BEPCII storage ring [33], which operates in the center-of-mass energy range from 2.0 GeV to 4.95 GeV. BESIII has collected large data

Table 2. Requirements on ΔE, ST yields, ST and DT efficiencies for the signal decays of $\Lambda_c^+ \to n\pi^+\pi^0$ ($\mathcal{E}$), $\Lambda_c^+ \to n\pi^+\pi^-\pi^+$ ($\mathcal{D}$) and $\Lambda_c^+ \to nK^-\pi^+\pi^+$ ($\mathcal{F}$) at $\sqrt{s} = 4681.92$ MeV. The uncertainties are statistical only. The quoted efficiencies do not include any subdecay BFs. Entries of "…" are for the cases where knowledge of the DT efficiencies is not required in the analysis.

Tag mode	ΔE /MeV	$N_i^{\rm ST}$	$\varepsilon_i^{\rm ST}(\%)$	$\varepsilon_i^{\rm DT}(\mathcal{E})(\%)$	$\varepsilon_i^{\rm DT}(\mathcal{D})(\%)$	$\varepsilon_i^{\rm DT}(\mathcal{F})(\%)$
$\bar{p}K_S^0$	$(-21, 18)$	3376±61	48.6	12.58	11.55	18.50
$\bar{p}K^+\pi^-$	$(-29, 26)$	17508±147	47.1	10.77	10.59	16.61
$\bar{p}K_S^0\pi^0$	$(-49, 34)$	1785±63	19.7	4.74	4.65	7.15
$\bar{p}K_S^0\pi^-\pi^+$	$(-34, 31)$	1511±57	20.7	4.22	4.13	5.99
$\bar{p}K^+\pi^-\pi^0$	$(-60, 41)$	5111±128	17.8	…	4.13	6.60
$\bar{\Lambda}\pi^-$	$(-23, 21)$	2074±48	41.3	9.95	9.12	15.08
$\bar{\Lambda}\pi^-\pi^0$	$(-50, 41)$	4380±88	18.2	4.05	3.85	6.00
$\bar{\Lambda}\pi^-\pi^+\pi^-$	$(-40, 36)$	2059±61	13.9	2.80	2.67	3.93
$\bar{\Sigma}^0\pi^-$	$(-33, 31)$	1398±42	25.9	6.31	5.89	8.46
$\bar{\Sigma}^-\pi^0$	$(-67, 32)$	879±43	22.5	5.78	5.21	8.22
$\bar{\Sigma}^-\pi^-\pi^+$	$(-40, 32)$	3027±88	22.1	5.40	5.21	7.77
$\bar{p}\pi^-\pi^+$	$(-26, 20)$	1596±80	53.6	…	…	17.35

samples in this energy region [34]. The cylindrical core of the BESIII detector covers 93% of the full solid angle and consists of a helium-based multilayer drift chamber (MDC), a plastic scintillator time-of-flight system (TOF), and a CsI(Tl) electromagnetic calorimeter (EMC), which are all enclosed in a superconducting solenoidal magnet providing a 1.0 T magnetic field. The solenoid is supported by an octagonal flux-return yoke with resistive plate counter muon identification modules interleaved with steel. The charged-particle momentum resolution at 1 GeV/c is 0.5%, and the specific ionization energy loss (dE/dx) resolution is 6% for electrons from Bhabha scattering. The EMC measures photon energies with a resolution of 2.5% (5%) at 1 GeV in the barrel (end-cap) region. The time resolution in the TOF barrel region is 68 ps, while that in the end-cap region is 60 ps [35–37]. High-statistics Monte Carlo (MC) simulation samples for the process $e^+e^- \to$ inclusive are produced with the KKMC generator [38] by incorporating the initial-state radiation (ISR) effects and the beam-energy spread. The inclusive MC simulation sample, which consists of $\Lambda_c^+\bar{\Lambda}_c^-$ events, $D_{(s)}^{(*)}$ production, ISR return to lower-mass ψ states, and continuum processes $e^+e^- \to q\bar{q}$ ($q = u,d,s$), is generated to determine the ST detection efficiencies and estimate the potential background. For this MC simulation sample, all the known decay modes of charmed hadrons and charmonia are modeled with evtgen [39, 40] using BFs taken from the PDG [23], and the remaining unknown decays are modeled with LUNDCHARM [41]. Furthermore, exclusive DT signal MC simulation events, where the $\bar{\Lambda}_c^-$ decays into any of the tag modes and the Λ_c^+ decays into any of the signal modes of $n\pi^+\pi^0$, $n\pi^+\pi^-\pi^+$ or $nK^-\pi^+\pi^+$, are used to determine the DT detection efficiencies. The Born cross sections are taken into account when producing the MC simulation sample of $\Lambda_c^+\bar{\Lambda}_c^-$ pairs. The $\Lambda_c^+ \to n\pi^+\pi^0$ and $\Lambda_c^+ \to n\pi^+\pi^-\pi^+$ signal MC samples are simulated evenly distributed in phase space since the angular distributions, momentum distributions and the two-body invariant mass distributions of the final state particles of the signal MC simulation samples are in good agreement with data with the current size of data set. For the signal MC simulation sample of $\Lambda_c^+ \to nK^-\pi^+\pi^+$, the key kinematic distributions mentioned above have been reweighted to agree with those of data. All final tracks and photons are fed into a GEANT4-based [42, 43] detector simulation package, which includes the geometric description of the BESIII detector.

III. ANALYSIS

Charged tracks detected in the MDC must satisfy $|\cos\theta| < 0.93$ (where θ is defined with respect to the z-axis, which is the symmetry axis of the MDC) and have a distance of closest approach to the interaction point (IP) of less than 10 cm along the beam axis and less than 1 cm in the perpendicular plane, except for those used for reconstructing K_S^0 and $\bar{\Lambda}$ decays. Particle identification (PID) for charged tracks combines measurements of the energy deposited in the MDC (dE/dx) and the flight time in the TOF to form likelihoods $\mathcal{L}(h)(h = p,K,\pi)$ for each hadron h hypothesis. Tracks are identified as protons when their likelihoods satisfy $\mathcal{L}(p) > \mathcal{L}(K)$ and $\mathcal{L}(p) > \mathcal{L}(\pi)$, while charged kaons and pions are identified by comparing the likelihoods for the kaon and pion hypotheses, $\mathcal{L}(K) > \mathcal{L}(\pi)$ or $\mathcal{L}(\pi) > \mathcal{L}(K)$, respectively.

Neutral showers are reconstructed in the EMC. Showers not associated with any charged track are identified as photon candidates. The deposited energy of each shower in the EMC must be greater than 25 MeV in the barrel region, corresponding to the polar angle $|\cos\theta| < 0.80$, and greater than 50 MeV in the end-cap region, corresponding to $0.86 < |\cos\theta| < 0.92$. The EMC time difference from the event start time is required to be less than 700 ns, to suppress electronic noise and showers unrelated to the event. The π^0 candidates are reconstructed from photon pairs with invariant masses within 115 MeV/c^2 < $M(\gamma\gamma)$ < 150 MeV/c^2. To improve momentum resolution, a kinematic fit constraining the photon pairs to the π^0 known mass is performed and the resulting four-momentum of the π^0 candidate is used for further analysis.

Candidates for K_S^0 and $\bar{\Lambda}$ decays are formed by $\pi^+\pi^-$ and $\bar{p}\pi^+$ combinations, respectively. For these tracks, their distances of closest approaches to the IP must be within ±20 cm along the beam direction. No distance constraint in the transverse plane is required. The charged pion is not subjected to the PID requirement described above, while the proton PID is imposed. The two final-state tracks are constrained to originate from a common decay vertex by requiring the χ^2 of the vertex fit to be less than 100. Furthermore, the decay vertex is required to be separated from the IP by a distance of at least twice the fitted vertex resolution. The fitted momenta of the $\pi^+\pi^-$ and $\bar{p}\pi^+$ combinations are used in the subsequent analysis. We require 487 MeV/c^2 < $M(\pi^+\pi^-)$ < 511 MeV/c^2 and 1111 MeV/c^2 < $M(\bar{p}\pi^+)$ < 1121 MeV/c^2 to select K_S^0 and $\bar{\Lambda}$ candidates, respectively, which corresponds to a window of about three times the standard deviations either side of the known masses. The $\bar{\Sigma}^0$ and $\bar{\Sigma}^-$ candidates are reconstructed with the $\gamma\bar{\Lambda}$ and $\bar{p}\pi^0$ combinations with invariant masses being in the intervals of 1179 MeV/c^2 < $M(\gamma\bar{\Lambda})$ < 1203 MeV/c^2 and 1176 MeV/c^2 < $M(\bar{p}\pi^0)$ < 1200 MeV/c^2, respectively.

For the tag modes $\bar{\Lambda}_c^- \to \bar{p}K_S^0\pi^0$, $\bar{\Lambda}_c^- \to \bar{p}K_S^0\pi^-\pi^+$, $\bar{\Lambda}_c^- \to \bar{\Sigma}^-\pi^-\pi^+$, and $\bar{\Lambda}_c^- \to \bar{p}\pi^-\pi^+$, possible backgrounds with $\bar{\Lambda} \to \bar{p}\pi^+$ are rejected by requiring $M(\bar{p}\pi^+)$ to be outside the range (1110, 1120) MeV/c^2. In the selection of $\bar{\Lambda}_c^- \to \bar{p}K_S^0\pi^0$ decays, candidate events within the range 1170 MeV/c^2 < $M(\bar{p}\pi^0)$ < 1200 MeV/c^2 are excluded to

suppress background from $\bar{\Sigma}^-$ decays. To remove K^0_S decays in the selection of $\bar{\Lambda}_c^- \to \bar{\Lambda}\pi^-\pi^+\pi^-$, $\bar{\Lambda}_c^- \to \bar{\Sigma}^-\pi^0$, $\bar{\Lambda}_c^- \to \bar{\Sigma}^-\pi^-\pi^+$, and $\bar{\Lambda}_c^- \to \bar{p}\pi^-\pi^+$ candidates, the invariant masses of any $\pi^+\pi^-$ and $\pi^0\pi^0$ pairs are required to lie outside of the range $(480,520)$ MeV/c^2. MC simulation studies indicate that peaking backgrounds and cross feeds among the twelve ST modes are negligible after applying the above veto procedures.

The ST $\bar{\Lambda}_c^-$ baryons are identified using the beam-constrained mass $M_{\rm BC} \equiv \sqrt{E^2_{\rm beam}/c^4 - p^2/c^2}$, where $E_{\rm beam}$ is the average value of the e^+ and e^- beam energies and p is the measured $\bar{\Lambda}_c^-$ momentum in the c.m. system of the e^+e^- collision. To improve the signal purity, the energy difference $\Delta E \equiv E - E_{\rm beam}$ for the $\bar{\Lambda}_c^-$ candidate is required to fulfil a mode-dependent ΔE requirement shown in Table 2, corresponding to approximately three times the resolutions. Here, E is the total reconstructed energy of the $\bar{\Lambda}_c^-$ candidate. For each ST mode, if more than one candidate satisfies the above requirements, we select the one with the minimal $|\Delta E|$. Figure 2 shows the $M_{\rm BC}$ distributions of various ST modes for the data sample at $\sqrt{s} = 4681.92$ MeV, where a clear $\bar{\Lambda}_c^-$ signal peak can be seen in each mode.

To obtain the ST yields, unbinned maximum-likelihood fits are performed to the $M_{\rm BC}$ distributions, where the signal shapes are modeled with the MC-simulated shape convolved with a Gaussian function representing the resolution difference between data and MC simulation, and the background shapes are described by an ARGUS function [44]. The fit results for the data sample at $\sqrt{s}$ =4681.92 MeV are shown in Fig. 2. The fits to the $M_{\rm BC}$ distributions for the other six data samples at different c.m. energies are shown in Appendix B. Candidates with $M_{\rm BC} \in (2275,2300)$ MeV/c^2 for the data sample at $\sqrt{s} = 4599.53$ MeV, $M_{\rm BC} \in (2275,2306)$ MeV/c^2 for the data samples at $\sqrt{s} =$ 4611.86 MeV, 4628.00 MeV, 4640.91 MeV, and $M_{\rm BC} \in (2275,2310)$ MeV/c^2 for the data samples at $\sqrt{s} =$ 4661.24 MeV, 4681.92 MeV, 4698.82 MeV are retained for further analysis. The differences in selection requirements between data sets are necessary as the resolution and effects of ISR vary with collision energy. The fitted ST yields, ST and DT efficiencies for each ST mode at $\sqrt{s} = 4681.92$ MeV are summarized in Table 2; those for the other c.m. energy points can be found in Appendix B.

Searches are performed for the decays $\Lambda_c^+ \to n\pi^+\pi^0$, $\Lambda_c^+ \to n\pi^+\pi^-\pi^+$ and $\Lambda_c^+ \to nK^-\pi^+\pi^+$ among the remaining tracks and showers recoiling against the ST $\bar{\Lambda}_c^-$ candidates. In the case of $\Lambda_c^+ \to n\pi^+\pi^0$, the event is allowed to contain only one pion with opposite charge to the tagged $\bar{\Lambda}_c^-$ satisfying the same selection criteria as described above. The π^0 candidate giving rise to the smallest χ^2 for the mass-constrained kinematic fit is retained. When searching for $\Lambda_c^+ \to n\pi^+\pi^-\pi^+$ and $\Lambda_c^+ \to nK^-\pi^+\pi^+$ decays,

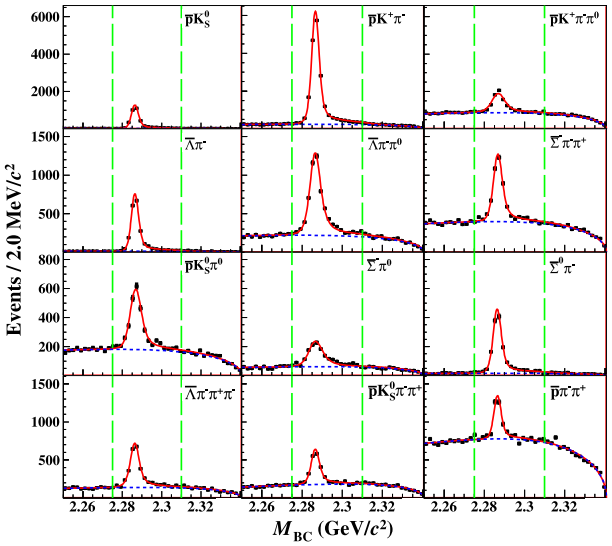


Fig. 2. (color online) The $M_{\rm BC}$ distributions of various ST modes for the data sample at $\sqrt{s}$=4681.92 MeV. The points with error bars represent data. The (red) solid curves indicate the fit results and the (blue) dashed curves describe the fitted background shapes. The ranges between green dashed lines are the signal regions.

events are selected with only three remaining charged tracks, satisfying the desired charge and PID criteria. In each of the decays, the kinematic variable $M_{\rm miss} \equiv \sqrt{E^2_{\rm miss}/c^4 - |\vec{p}_{\rm miss}|^2/c^2}$ is used to infer the presence of the undetected neutron. Here, $E_{\rm miss}$ and $\vec{p}_{\rm miss}$ are calculated by $E_{\rm miss} \equiv E_{\rm beam} - E_{\rm rec}$ and $\vec{p}_{\rm miss} \equiv \vec{p}_{\Lambda_c^+} - \vec{p}_{\rm rec}$, where $E_{\rm rec}(\vec{p}_{\rm rec})$ is the energy (momentum) of the reconstructed final-state particles in the e^+e^- c.m. system. The momentum of the Λ_c^+ baryon $\vec{p}_{\Lambda_c^+}$ is calculated by $\vec{p}_{\Lambda_c^+} \equiv -\hat{p}_{\rm tag}\sqrt{E^2_{\rm beam}/c^2 - m^2_{\Lambda_c^+}c^2}$, where $\hat{p}_{\rm tag}$ is the momentum direction of the ST $\bar{\Lambda}_c^-$ and $m_{\Lambda_c^+}$ is the known mass of the Λ_c^+ baryon [23]. In the case of $\Lambda_c^+ \to n\pi^+\pi^0$, $\Lambda_c^+ \to n\pi^+\pi^-\pi^+$, and $\Lambda_c^+ \to nK^-\pi^+\pi^+$ decays, the $M_{\rm miss}(\pi^+\pi^0)$, $M_{\rm miss}(\pi^+\pi^-\pi^+)$ and $M_{\rm miss}(K^-\pi^+\pi^+)$ spectra are expected to peak around the known mass of the neutron *i.e.* at 939.6 MeV/c^2 [23]. A study of the inclusive MC simulation sample reveals that the dominant background events for the signal mode $\Lambda_c^+ \to n\pi^+\pi^0$ are from the processes $\Lambda_c^+ \to \Lambda\pi^+$ with $\Lambda \to n\pi^0$, $\Lambda_c^+ \to \Sigma^+\pi^0$ with $\Sigma^+ \to n\pi^+$ and $\Lambda_c^+ \to \Sigma^0\pi^+$ with $\Sigma^0 \to \gamma\Lambda(\to n\pi^0)$. In order to reject these background events for $\Lambda_c^+ \to n\pi^+\pi^0$, the following selection criteria are applied: $M_{\rm miss}(\pi^+) > 1300$ MeV/c^2 and $M_{\rm miss}(\pi^0) > 1370$ MeV/c^2. For the signal mode $\Lambda_c^+ \to n\pi^+\pi^-\pi^+$, the peaking backgrounds from the decays $\Lambda_c^+ \to nK^0_S(\to \pi^+\pi^-)\pi^+$, $\Lambda_c^+ \to \Sigma^+(\to n\pi^+)\pi^+\pi^-$, and $\Lambda_c^+ \to \Sigma^-(\to n\pi^-)\pi^+\pi^+$ are suppressed by requiring $M_{\pi^+\pi^-} \notin (487,511)$ MeV/c^2, $M_{\rm miss}(\pi^+\pi^-) \notin (1150,1250)$ MeV/c^2 and $M_{\rm miss}(\pi^+\pi^+) \notin (1150,1250)$ MeV/c^2. Note that, based on the study of the inclusive MC simulation

sample, ten ST modes (after excluding $\bar{\Lambda}_c^- \to \bar{p}K^+\pi^-\pi^0$ and $\bar{\Lambda}_c^- \to \bar{p}\pi^-\pi^+$) are used in the analysis of the decay $\Lambda_c^+ \to n\pi^+\pi^0$, and eleven ST modes (after excluding $\bar{\Lambda}_c^- \to \bar{p}\pi^-\pi^+$) are used in the analysis of the decay $\Lambda_c^+ \to n\pi^+\pi^-\pi^+$ to improve the background level in the $M_{\rm miss}$ spectra.

The resulting $M_{\rm miss}$ distributions of the DT candidate events summed over all data samples at seven c.m. energies are shown in Fig. 3. A peak around the neutron mass is observed in Fig. 3(a) representing the $\Lambda_c^+ \to n\pi^+\pi^0$ signal. Moreover, there are two prominent structures peaking around the Λ and Σ^0 mass regions, which correspond to the CF decays $\Lambda_c^+ \to \Lambda\pi^+\pi^0$ and $\Lambda_c^+ \to \Sigma^0\pi^+\pi^0$, respectively. Significant signal peaks around the neutron mass are also observed for $\Lambda_c^+ \to n\pi^+\pi^-\pi^+$ and $\Lambda_c^+ \to nK^-\pi^+\pi^+$ in Fig. 3(b) and Fig. 3(c), respectively.

The total DT signal yield is obtained by performing an unbinned maximum-likelihood fit on the $M_{\rm miss}$ distribution. The neutron, Λ and Σ^0 signals are modeled by individual MC-derived shapes convolved with Gaussian functions that account for the shift and resolution difference between data and MC simulation. The Gaussian-function parameters are left free and are shared by the three signal processes in the fit to the $M_{\rm miss}(\pi^+\pi^0)$ spectra. The potential background events in the $M_{\rm miss}$ distributions are classified into two categories. Those directly originating from continuum hadron production in the e^+e^- annihilation are denoted as $q\bar{q}$ background. Those from $e^+e^- \to \Lambda_c^+\bar{\Lambda}_c^-$ events excluding the contributions from the corresponding signal process are referred to as $\Lambda_c^+\bar{\Lambda}_c^-$ background. In the fit to the $M_{\rm miss}(\pi^+\pi^0)$ distribution, the $q\bar{q}$ background is described by a second-order Chebyshev polynomial with free parameters and the $\Lambda_c^+\bar{\Lambda}_c^-$ backgroud shape is taken from the inclusive MC simulation sample. For the fit to the $M_{\rm miss}(\pi^+\pi^-\pi^+)$ spectrum, only one first-order Chebyshev polynomial with free parameters is used to model all the background. Similarly, for the $M_{\rm miss}(K^-\pi^+\pi^+)$ distribution, one second-order Chebyshev function with fixed parameters is taken as the background shape where the parameters are derived from the fit to the inclusive MC simulation sample. The DT signal and background yields are left free in the fit to

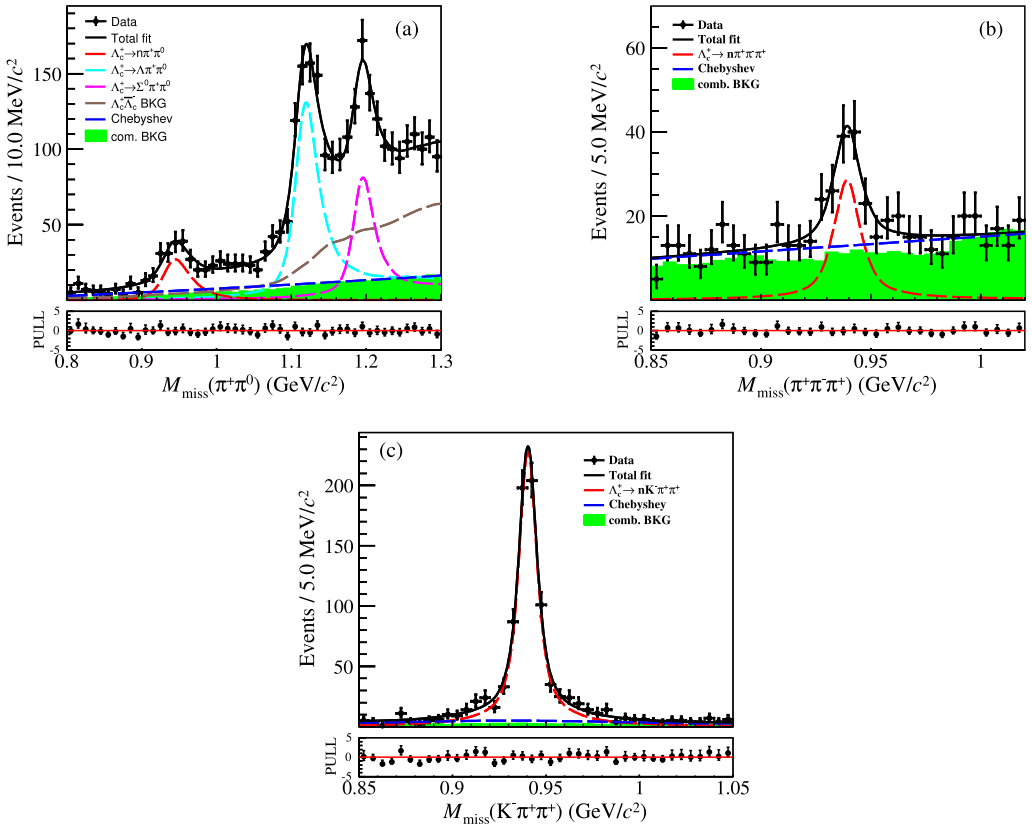


Fig. 3. (color online) The $M_{\rm miss}$ distributions of the surviving DT candidate events for (a) $\Lambda_c^+ \to n\pi^+\pi^0$, (b) $\Lambda_c^+ \to n\pi^+\pi^-\pi^+$ and (c) $\Lambda_c^+ \to nK^-\pi^+\pi^+$ decays with fit results overlaid. The points with error bars are data combined from seven c.m. energy points. The solid black curves are the fit results. The red, cyan, and pink dashed curves indicate the neutron, Λ, and Σ signal shapes, respectively. The brown dashed curve is the $\Lambda_c^+\bar{\Lambda}_c^-$ background shape for $\Lambda_c^+ \to n\pi^+\pi^0$. The blue dashed curves represent the fitted combinatorial background shape. The green histograms are the simulated combinatorial background shapes from the inclusive MC sample. The plots in the bottom of each graphs show the pull value of each bin, in which the values are expected to fluctuate around 0.

the $M_{\rm miss}(\pi^+\pi^0)$, $M_{\rm miss}(\pi^+\pi^-\pi^+)$ and $M_{\rm miss}(K^-\pi^+\pi^+)$ spectra. Figure 3 shows the results of the fits to the $M_{\rm miss}$ distributions. From these fits, we determine the DT signal yields of $\Lambda_c^+\to n\pi^+\pi^0$, $\Lambda_c^+\to n\pi^+\pi^-\pi^+$, and $\Lambda_c^+\to nK^-\pi^+\pi^+$ to be $N^{\rm DT}_{n\pi^+\pi^0}=150.9\pm21.4$, $N^{\rm DT}_{n\pi^+\pi^-\pi^+}=120.6\pm17.9$ and $N^{\rm DT}_{nK^-\pi^+\pi^+}=805.8\pm33.1$, respectively, where the uncertainties are statistical only. The statistical significances of the $\Lambda_c^+\to n\pi^+\pi^0$, $\Lambda_c^+\to n\pi^+\pi^-\pi^+$ and $\Lambda_c^+\to nK^-\pi^+\pi^+$ signals are 7.9σ, 7.8σ, and $>10\sigma$, respectively, which are evaluated by the changes in the likelihoods between the nominal fit and the fit with the signal yield set to zero, and accounting for the change in the number of degrees of freedom.

The BFs of the decays $\Lambda_c^+\to n\pi^+\pi^0$, $\Lambda_c^+\to n\pi^+\pi^-\pi^+$, and $\Lambda_c^+\to nK^-\pi^+\pi^+$ are determined as

$$\mathcal{B}=\frac{N^{\rm DT}}{\sum_{ij}N^{\rm ST}_{ij}\cdot(\epsilon^{\rm DT}_{ij}/\epsilon^{\rm ST}_{ij})\cdot\mathcal{B}_{\rm int}}, \quad (1)$$

where i and j represent the ST modes and the data samples at different c.m. energies, respectively. The factor $\mathcal{B}_{\rm int}$ is $(98.823\pm0.034)\,\%$, which is the BF of $\pi^0\to\gamma\gamma$ [23], is only present for $\Lambda_c^+\to n\pi^+\pi^0$. $N^{\rm ST}_{ij}$, $\epsilon^{\rm ST}_{ij}$, and $\epsilon^{\rm DT}_{ij}$ are the ST yields, ST efficiencies, and DT efficiencies, respectively. The detection efficiencies $\epsilon^{\rm ST}_{ij}$ and $\epsilon^{\rm DT}_{ij}$ are estimated from the inclusive MC simulation sample and exclusive DT signal MC simulation samples, respectively. The ST and DT efficiencies for the data sample at $\sqrt{s}=4681.92$ MeV are summarized in Table 2. The detection efficiencies for the other data samples are summarized in Appendix B. The obtained BFs are summaried in Table 3.

Most systematic uncertainties from the ST side cancel in the determination of the BFs, as is clear from Eq. (1). However, effects from the signal side can lead to systematic bias, for example, the requirement of no extra charged track, tracking efficiency, PID efficiency, π^0 reconstruction, peaking background veto, $M_{\rm miss}$ fit, ST $\bar{\Lambda}_c^-$ yield, MC modeling, and MC sample size. The systematic uncertainty due to the requirement of no extra charged track is assigned as 1.1% from the study of a control sample of $e^+e^-\to\Lambda_c^+\bar{\Lambda}_c^-$ with $\Lambda_c^+\to nK^-\pi^+\pi^+$ and $\bar{\Lambda}_c^-$ decays to tag modes. The systematic uncertainties associated with the efficiencies of the tracking and PID of charged particles are estimated to be 1% by using control samples of $e^+e^-\to\pi^+\pi^+\pi^-\pi^-$ and $e^+e^-\to K^+K^-\pi^+\pi^-$ events collected at c.m. energies above $\sqrt{s}=4.0\,$GeV. The systematic uncertainty due to the π^0 reconstruction efficiency is assigned to be 1.0% [12]. The systematic uncertainty associated with the BF of $\pi^0\to\gamma\gamma$ is 0.03% [23], which is negligible. In order to estimate the systematic uncertainties arising from the veto of peaking backgrounds involving Λ, Σ^+, Σ^0, K^0_S, and Σ^-, the corresponding resolutions in the MC simulation samples are corrected to agree with those in data, and the BFs are then re-evaluated with the updated MC simulation samples. The deviations from the baseline BF measurements are taken as the associated systematic uncertainties for $\Lambda_c^+\to n\pi^+\pi^0$ and $\Lambda_c^+\to n\pi^+\pi^-\pi^+$, which are 1.6% and 1.0%, respectively. The systematic uncertainties from the fitted DT yields are 1.3%, 2.2%, and 0.9% for $\Lambda_c^+\to n\pi^+\pi^0$, $n\pi^+\pi^-\pi^+$, and $nK^-\pi^+\pi^+$, respectively, which are estimated from varying the alternative polynomial descriptions for the $q\bar{q}$ and $\Lambda_c^+\bar{\Lambda}_c^-$ backgrounds, respectively. The systematic uncertainty in the total ST $\bar{\Lambda}_c^-$ yield is 0.1% for $\Lambda_c^+\to n\pi^+\pi^0$, and 0.2% for $\Lambda_c^+\to n\pi^+\pi^-\pi^+$, and $nK^-\pi^+\pi^+$. These uncertainties arise from the fluctuation of background together with a component coming from the fit to the $M_{\rm BC}$ distribution. The systematic uncertainties arising from the MC modeling are investigated by reweighting the MC distribution to data, and they are assigned as the efficiency differences between the original and reweighted samples. The systematic uncertainties due to limited sample sizes of the MC samples are estimated to be 0.2%. Assuming that all the sources are uncorrelated, the total uncertainties are then taken to be the quadratic sums of the individual values, which are 3.1%, 5.6%, and 4.5% for $\Lambda_c^+\to n\pi^+\pi^0$, $\Lambda_c^+\to n\pi^+\pi^-\pi^+$, and $\Lambda_c^+\to nK^-\pi^+\pi^+$, respectively. All the above systematic uncertainties are summarized in Table 4.

Table 3. The obtained BFs, where the first uncertainties are statistical and the second are systematic.

Signal decay	$\mathcal{B}$ (%)
$\Lambda_c^+\to n\pi^+\pi^0$	$0.64\pm0.09\pm0.02$
$\Lambda_c^+\to n\pi^+\pi^-\pi^+$	$0.45\pm0.07\pm0.03$
$\Lambda_c^+\to nK^-\pi^+\pi^+$	$1.90\pm0.08\pm0.09$

Table 4. Relative systematic uncertainties in BF measurements. "…" means the uncertainty is negligible. "–" indicates cases where there is no uncertainty.

Source	$n\pi^+\pi^0$ (%)	$n\pi^+\pi^-\pi^+$ (%)	$nK^-\pi^+\pi^+$ (%)
No extra charged track	1.1	1.1	1.1
Tracking	1.0	3.0	3.0
PID	1.0	3.0	3.0
π^0 reconstruction	1.0	–	–
Background veto	1.6	1.0	–
$M_{\rm miss}$ fit	1.3	2.2	0.9
ST $\bar{\Lambda}_c^-$ yield	0.1	0.2	0.2
MC model	1.1	2.6	…
MC sample size	0.2	0.2	0.2
Total	3.1	5.6	4.5

IV. SUMMARY

In summary, by analyzing 4.5 fb^{-1} of data collected at c.m. energies between 4599.53 and 4698.82 MeV, we report for the first time the observation of $\Lambda_c^+ \to n\pi^+\pi^0$, $\Lambda_c^+ \to n\pi^+\pi^-\pi^+$ and $\Lambda_c^+ \to nK^-\pi^+\pi^+$. The BFs of these decays are determined to be $\mathcal{B}(\Lambda_c^+ \to n\pi^+\pi^0) = (0.64\pm 0.09 \pm 0.02)\%$, $\mathcal{B}(\Lambda_c^+ \to n\pi^+\pi^-\pi^+) = (0.45 \pm 0.07 \pm 0.03)\%$, and $\mathcal{B}(\Lambda_c^+ \to nK^-\pi^+\pi^+) = (1.90 \pm 0.08 \pm 0.09)\%$, where the first uncertainties are statistical and the second systematic. These observations are important additions to our knowledge of Λ_c^+ decays. Comparison of these results to those of decays involving protons provides crucial inputs for understanding the mechanisms in the charmed baryon decays under the $SU(3)$ flavor symmetry. Taking $\mathcal{B}(\Lambda_c^+ \to p\pi^-\pi^+) = (0.461 \pm 0.028)\%$ from the PDG [23], we can calculate $\mathcal{B}(\Lambda_c^+ \to p\pi^-\pi^+)/\mathcal{B}(\Lambda_c^+ \to n\pi^0\pi^+) = 0.72\pm 0.11$. This result provides useful input to test of isospin symmetry in the charm baryon sector. Taking $\mathcal{B}(\Lambda_c^+ \to n\pi^+) = (6.6 \pm 1.3)\times 10^{-4}$ [18], the ratio $\mathcal{B}(\Lambda_c^+ \to n\pi^+\pi^0)/\mathcal{B}(\Lambda_c^+ \to n\pi^+)$ is calculated to be 9.7 ± 2.4, indicating an order-of-magnitude difference in the rates of the two decays. This ratio is greater than $\mathcal{B}(\Lambda_c^+ \to pK_S^0\pi^0)/\mathcal{B}(\Lambda_c^+ \to pK_S^0) = (1.24 \pm 0.10)$. To further understand this behavior, amplitude analysis will be needed to decouple the intermediate resonances contributions for $\Lambda_c^+ \to n\pi^+\pi^0$ and $\Lambda_c^+ \to pK_S^0\pi^0$. The ratio of $\mathcal{B}(\Lambda_c^+ \to n\pi^+\pi^-\pi^+)/\mathcal{B}(\Lambda_c^+ \to nK^-\pi^+\pi^+) = (0.24 \pm 0.04)$ which is consistent with the ratio of Cabibbo-Kobayashi-Maskawa matrix elements $|V_{cd}|/|V_{cs}| = (0.224 \pm 0.005)$ offers a new constraint on the CS and CF decay dynamics. The results from this analysis provide an essential input for the phenomenological studies on the underlying dynamics of charmed bayond decays.

ACKNOWLEDGEMENTS

The BESIII collaboration thanks the staff of BEPCII and the IHEP computing center for their strong support. The authors are grateful to Fusheng Yu for enlightening discussions.

APPENDIX A

Figures A1 and A2 show the topological diagrams of $\Lambda_c^+ \to n\pi^+\pi^-\pi^+$ and $\Lambda_c^+ \to nK^-\pi^+\pi^+$, respectively.

APPENDIX B

Figures B1–B6 show the fits for the $M_{\rm BC}$ distributions of the ST $\bar{\Lambda}_c^-$ candidates for various tag modes from the data samples at $\sqrt{s}$ = 4599.53, 4611.86, 4628.00, 4640.91, 4661.24, and 4698.82 MeV, respectively.

Tables B1–B6 show the ST yields, ST and DT efficiencies for various tag modes from the data samples at $\sqrt{s}$ = 4599.53, 4611.86, 4628.00, 4640.91, 4661.24, and 4698.82 MeV, respectively.

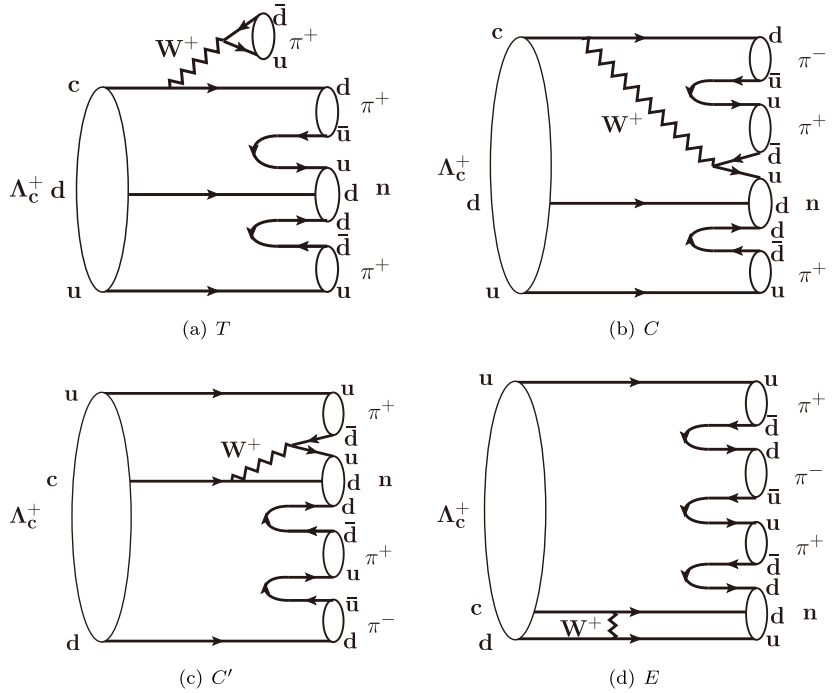


Fig. A1. Topological diagrams of $\Lambda_c^+ \to n\pi^+\pi^-\pi^+$ via (a) external W-emission T, (b) internal W-emission C, (c) inner W-emission C', and (d) W-exchange diagram E.

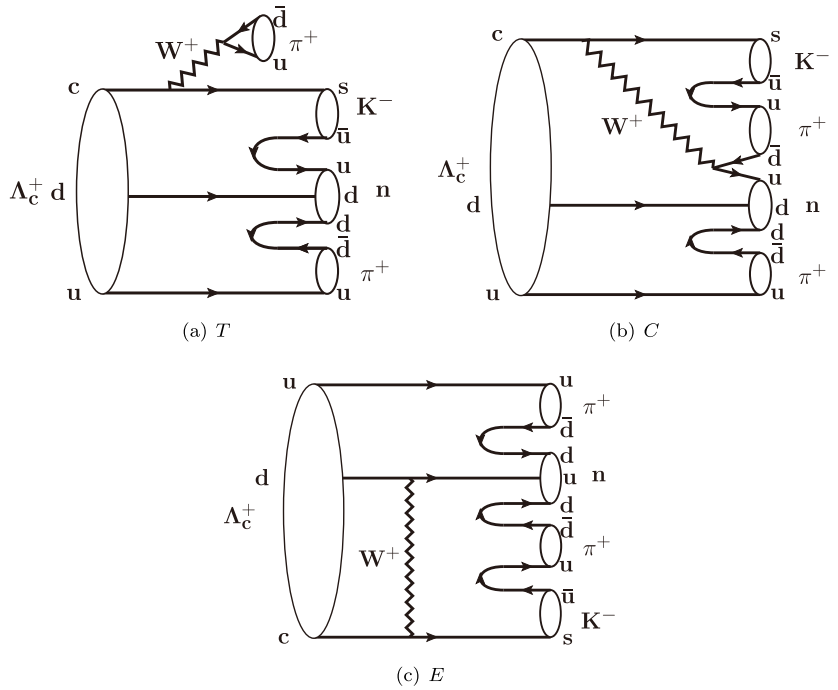


Fig. A2. Topological diagrams of $\Lambda_c^+ \to nK^-\pi^+\pi^+$ via (a) external W-emission T, (b) internal W-emission C, (c) W-exchange diagram E.

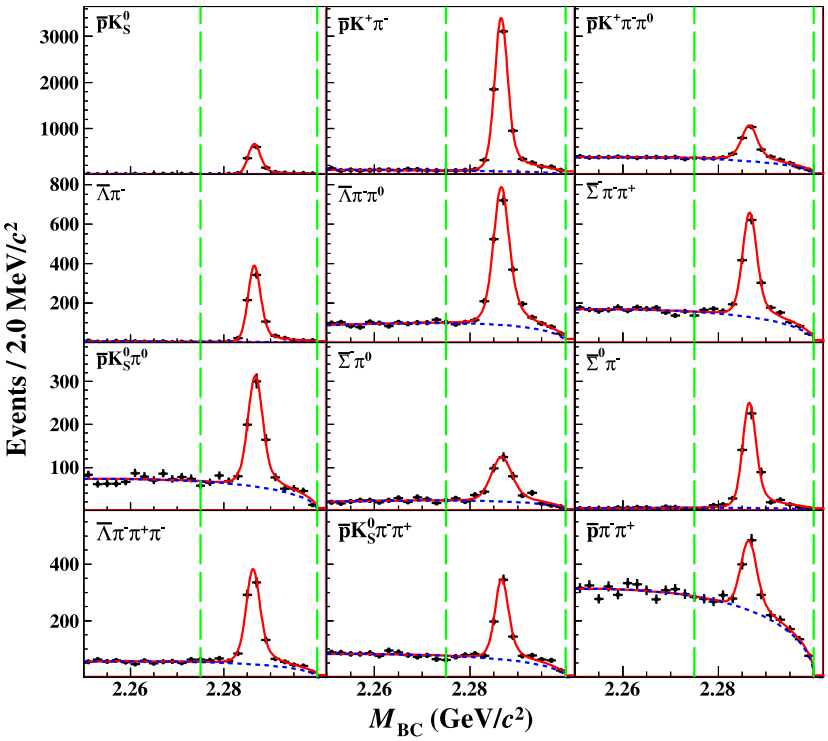


Fig. B1. (color online) The $M_{\rm BC}$ distributions of the ST $\bar{\Lambda}_c^-$ candidates of various tag modes for the data sample at $\sqrt{s} = 4599.53$ MeV. The points with error bars represent data. The red solid curves indicate the fit results and the blue dashed curves describe the background shapes. The ranges between green dashed lines are the signal regions.

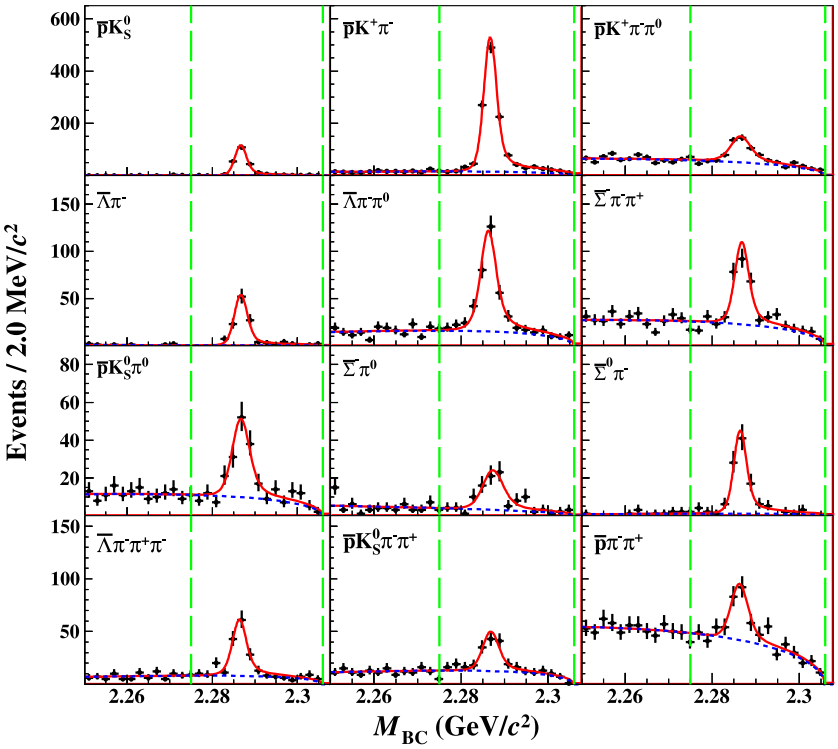


Fig. B2. (color online) The $M_{\rm BC}$ distributions of the ST $\bar{\Lambda}_c^-$ candidates of various tag modes for the data sample at $\sqrt{s} = 4611.86$ MeV. The points with error bars represent data. The red solid curves indicate the fit results and the blue dashed curves describe the background shapes. The ranges between green dashed lines are the signal regions.

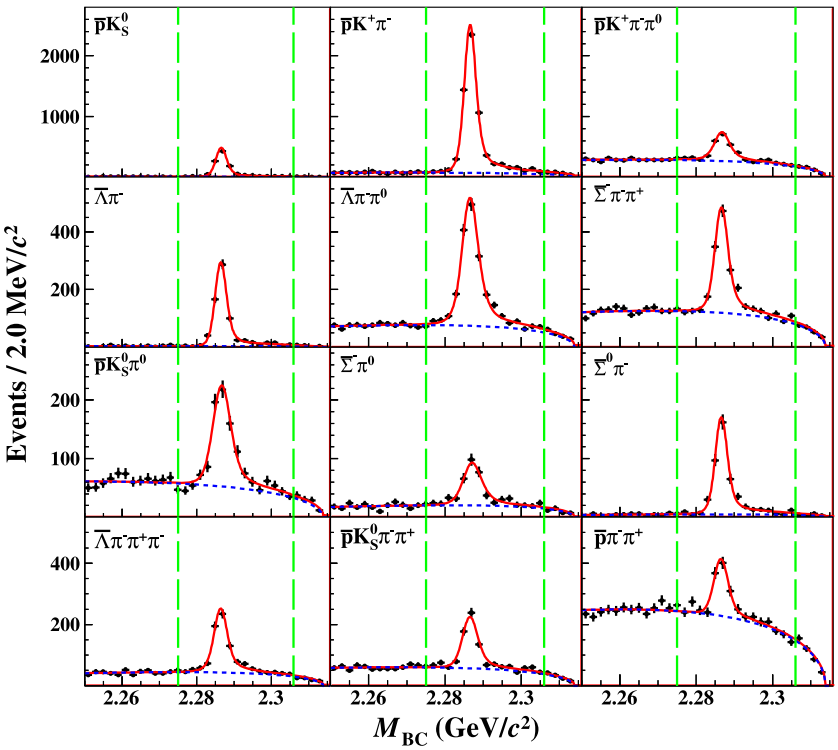


Fig. B3. (color online) The $M_{\rm BC}$ distributions of the ST $\bar{\Lambda}_c^-$ candidates of various tag modes for the data sample at $\sqrt{s} = 4628.00$ MeV. The points with error bars represent data. The red solid curves indicate the fit results and the blue dashed curves describe the background shapes. The ranges between green dashed lines are the signal regions.

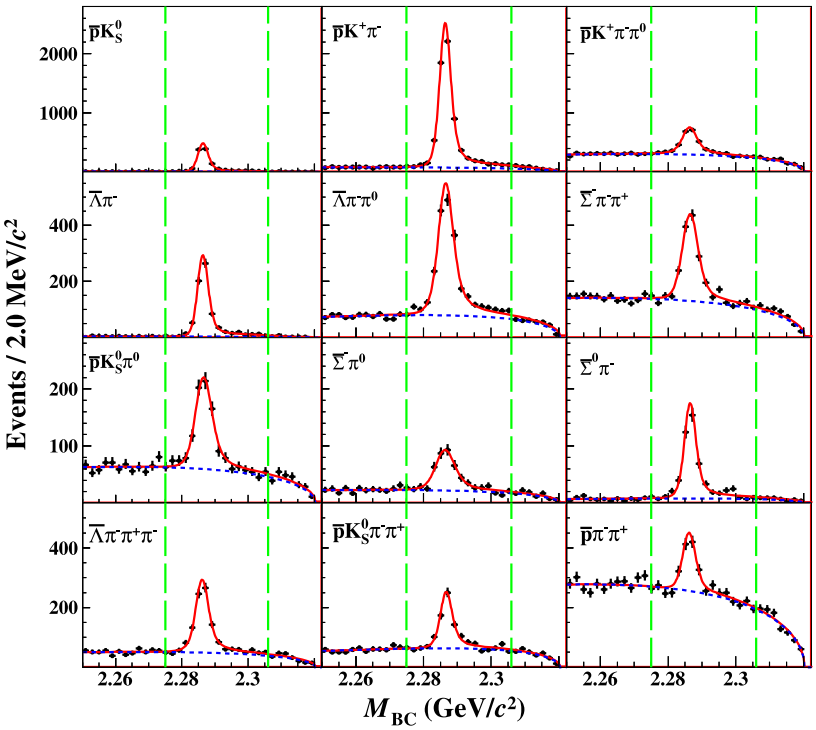


Fig. B4. (color online) The $M_{\rm BC}$ distributions of the ST $\bar{\Lambda}_c^-$ candidates of various tag modes for the data sample at $\sqrt{s} = 4640.91$ MeV. The points with error bars represent data. The red solid curves indicate the fit results and the blue dashed curves describe the background shapes. The ranges between green dashed lines are the signal regions.

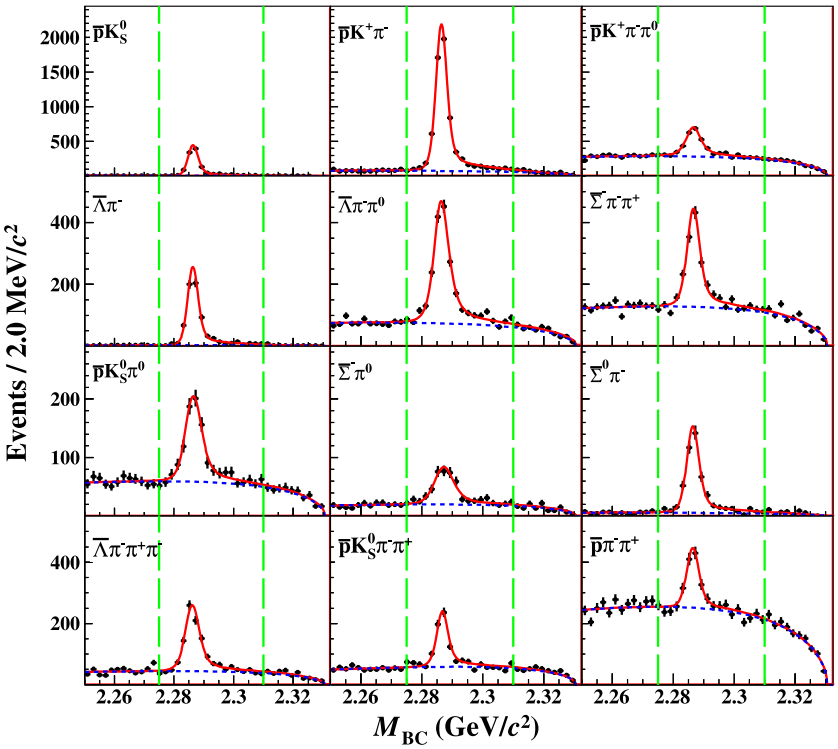


Fig. B5. (color online) The $M_{\rm BC}$ distributions of the ST $\bar{\Lambda}_c^-$ candidates of various tag modes for the data sample at $\sqrt{s} = 4661.24$ MeV. The points with error bars represent data. The red solid curves indicate the fit results and the blue dashed curves describe the background shapes. The ranges between green dashed lines are the signal regions.

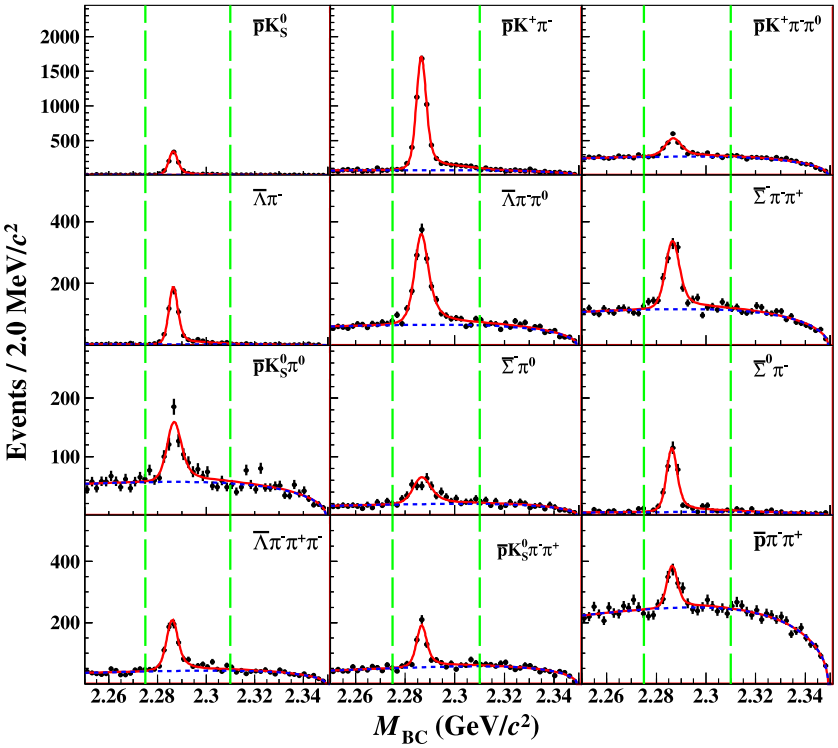


Fig. B6. (color online) The $M_{\rm BC}$ distributions of the ST $\bar{\Lambda}_c^-$ candidates of various tag modes for the data sample at $\sqrt{s} = 4698.82$ MeV. The points with error bars represent data. The red solid curves indicate the fit results and the blue dashed curves describe the background shapes. The ranges between green dashed lines are the signal regions.

Table B1. ST yields, ST and DT efficiencies of various tag modes for the data sample at $\sqrt{s} = 4599.53$ MeV. The uncertainties are statistical only. The quoted efficiencies do not include any subdecay BFs. Entries of "…" are for the cases where knowledge of the DT efficiencies are not required in the analysis.

Tag mode	$N_i^{\rm ST}$	$\varepsilon_i^{\rm ST}(\%)$	$\varepsilon_i^{\rm DT}(n\pi^+\pi^0)(\%)$	$\varepsilon_i^{\rm DT}(n\pi^+\pi^-\pi^+)(\%)$	$\varepsilon_i^{\rm DT}(nK^-\pi^+\pi^-)(\%)$
$\bar{p}K_S^0$	1277 ± 36	56.1	14.27	13.49	20.87
$\bar{p}K^+\pi^-$	6806 ± 91	51.5	11.25	11.53	17.64
$\bar{p}K_S^0\pi^0$	606 ± 34	23.0	5.17	5.25	7.34
$\bar{p}K_S^0\pi^-\pi^+$	613 ± 34	23.5	4.51	4.76	6.89
$\bar{p}K^+\pi^-\pi^0$	2197 ± 78	20.6	…	4.57	6.83
$\bar{\Lambda}\pi^-$	757 ± 28	48.4	11.62	10.9	17.08
$\bar{\Lambda}\pi^-\pi^0$	1742 ± 56	21.6	4.52	4.43	6.42
$\bar{\Lambda}\pi^-\pi^+\pi^-$	769 ± 36	15.6	2.86	2.90	4.17
$\bar{\Sigma}^0\pi^-$	520 ± 26	29.4	7.30	6.96	11.20
$\bar{\Sigma}^-\pi^0$	320 ± 25	23.7	6.47	6.05	8.38
$\bar{\Sigma}^-\pi^-\pi^+$	1186 ± 49	25.4	5.84	5.82	8.81
$\bar{p}\pi^-\pi^+$	598 ± 47	64.3	…	…	22.04

Table B2. ST yields, ST and DT efficiencies of various tag modes for the data sample at $\sqrt{s} = 4611.86\,\text{MeV}$. The uncertainties are statistical only. The quoted efficiencies do not include any subdecay BFs. Entries of "⋯" are for the cases where knowledge of the DT efficiencies are not required in the analysis.

Tag mode	$N_i^{\rm ST}$	$\varepsilon_i^{\rm ST}(\%)$	$\varepsilon_i^{\rm DT}(n\pi^+\pi^0)(\%)$	$\varepsilon_i^{\rm DT}(n\pi^+\pi^-\pi^+)(\%)$	$\varepsilon_i^{\rm DT}(nK^-\pi^+\pi^-)(\%)$
$\bar{p}K_S^0$	239 ± 16	53.7	13.89	12.71	20.09
$\bar{p}K^+\pi^-$	1166 ± 39	51.0	11.34	11.27	16.98
$\bar{p}K_S^0\pi^0$	127 ± 17	22.2	5.04	4.91	7.20
$\bar{p}K_S^0\pi^-\pi^+$	106 ± 16	21.9	4.35	4.33	6.04
$\bar{p}K^+\pi^-\pi^0$	364 ± 34	19.9	⋯	4.40	6.25
$\bar{\Lambda}\pi^-$	123 ± 11	46.9	11.29	10.22	15.27
$\bar{\Lambda}\pi^-\pi^0$	302 ± 23	19.8	4.34	4.17	6.08
$\bar{\Lambda}\pi^-\pi^+\pi^-$	139 ± 15	13.6	2.68	2.75	3.69
$\bar{\Sigma}^0\pi^-$	102 ± 13	26.6	6.89	6.53	8.65
$\bar{\Sigma}^-\pi^0$	73 ± 10	22.6	6.47	5.9	8.46
$\bar{\Sigma}^-\pi^-\pi^+$	218 ± 22	25.5	5.74	5.63	8.47
$\bar{p}\pi^-\pi^+$	155 ± 22	71.4	⋯	⋯	21.82

Table B3. ST yields, ST and DT efficiencies of various tag modes for the data sample at $\sqrt{s} = 4628.00\,\text{MeV}$. The uncertainties are statistical only. The quoted efficiencies do not include any subdecay BFs.Entries of "⋯" are for the cases where knowledge of the DT efficiencies are not required in the analysis.

Tag mode	$N_i^{\rm ST}$	$\varepsilon_i^{\rm ST}(\%)$	$\varepsilon_i^{\rm DT}(n\pi^+\pi^0)(\%)$	$\varepsilon_i^{\rm DT}(n\pi^+\pi^-\pi^+)(\%)$	$\varepsilon_i^{\rm DT}(nK^-\pi^+\pi^-)(\%)$
$\bar{p}K_S^0$	1054 ± 35	51.8	13.27	12.17	18.98
$\bar{p}K^+\pi^-$	5886 ± 39	49.2	10.98	10.97	16.77
$\bar{p}K_S^0\pi^0$	616 ± 36	20.7	4.94	4.79	6.73
$\bar{p}K_S^0\pi^-\pi^+$	510 ± 32	20.6	4.21	4.17	6.01
$\bar{p}K^+\pi^-\pi^0$	1589 ± 69	18.7	⋯	4.32	6.95
$\bar{\Lambda}\pi^-$	675 ± 28	43.2	10.69	9.84	14.72
$\bar{\Lambda}\pi^-\pi^0$	1454 ± 54	19.1	4.18	3.98	5.90
$\bar{\Lambda}\pi^-\pi^+\pi^-$	587 ± 33	13.6	2.70	2.65	3.67
$\bar{\Sigma}^0\pi^-$	413 ± 23	27.2	6.62	6.24	8.41
$\bar{\Sigma}^-\pi^0$	263 ± 23	23.4	6.20	5.65	9.10
$\bar{\Sigma}^-\pi^-\pi^+$	994 ± 20	23.6	5.54	5.47	8.24
$\bar{p}\pi^-\pi^+$	517 ± 45	61.6	⋯	⋯	19.75

Table B4. ST yields, ST and DT efficiencies of various tag modes for the data sample at $\sqrt{s} = 4640.91\,\text{MeV}$. The uncertainties are statistical only. The quoted efficiencies do not include any subdecay BFs. Entries of "⋯" are for the cases where knowledge of the DT efficiencies are not required in the analysis.

Tag mode	$N_i^{\rm ST}$	$\varepsilon_i^{\rm ST}(\%)$	$\varepsilon_i^{\rm DT}(n\pi^+\pi^0)(\%)$	$\varepsilon_i^{\rm DT}(n\pi^+\pi^-\pi^+)(\%)$	$\varepsilon_i^{\rm DT}(nK^-\pi^+\pi^-)(\%)$
$\bar{p}K_S^0$	1107 ± 36	50.7	13.14	12.08	19.12
$\bar{p}K^+\pi^-$	6250 ± 89	48.5	10.91	10.86	16.83
$\bar{p}K_S^0\pi^0$	599 ± 36	20.7	4.82	4.77	7.02
$\bar{p}K_S^0\pi^-\pi^+$	522 ± 33	20.8	4.21	4.15	6.50
$\bar{p}K^+\pi^-\pi^0$	1632 ± 70	18.1	⋯	4.23	6.62
$\bar{\Lambda}\pi^-$	705 ± 29	42.7	10.51	9.55	14.24
$\bar{\Lambda}\pi^-\pi^0$	1613 ± 54	19.1	4.14	3.95	5.46
$\bar{\Lambda}\pi^-\pi^+\pi^-$	745 ± 36	14.2	2.70	2.67	4.20
$\bar{\Sigma}^0\pi^-$	445 ± 25	26.2	6.43	6.09	8.97
$\bar{\Sigma}^-\pi^0$	298 ± 24	24.6	6.01	5.52	7.70
$\bar{\Sigma}^-\pi^-\pi^+$	1077 ± 49	23.4	5.43	5.38	8.01
$\bar{p}\pi^-\pi^+$	552 ± 47	59.7	⋯	⋯	22.97

Table B5. ST yields, ST and DT efficiencies of various tag modes for the data sample at $\sqrt{s} = 4661.24\,\text{MeV}$. The uncertainties are statistical only. The quoted efficiencies do not include any subdecay BFs. Entries of "⋯" are for the cases where knowledge of the DT efficiencies are not required in the analysis.

Tag mode	$N_i^{\rm ST}$	$\varepsilon_i^{\rm ST}(\%)$	$\varepsilon_i^{\rm DT}(n\pi^+\pi^0)(\%)$	$\varepsilon_i^{\rm DT}(n\pi^+\pi^-\pi^+)(\%)$	$\varepsilon_i^{\rm DT}(nK^-\pi^+\pi^-)(\%)$
$\bar{p}K_S^0$	1119 ± 35	49.6	12.82	11.78	18.58
$\bar{p}K^+\pi^-$	5938 ± 86	48.2	10.93	10.85	16.47
$\bar{p}K_S^0\pi^0$	594 ± 36	20.1	4.86	4.75	7.12
$\bar{p}K_S^0\pi^-\pi^+$	537 ± 33	20.2	4.29	4.17	6.27
$\bar{p}K^+\pi^-\pi^0$	1700 ± 73	18.1	⋯	4.15	6.36
$\bar{\Lambda}\pi^-$	668 ± 27	41.7	10.15	9.41	14.98
$\bar{\Lambda}\pi^-\pi^0$	1491 ± 51	18.9	4.15	3.91	5.91
$\bar{\Lambda}\pi^-\pi^+\pi^-$	780 ± 36	14.1	2.71	2.63	4.04
$\bar{\Sigma}^0\pi^-$	454 ± 25	26.3	6.56	5.94	9.20
$\bar{\Sigma}^-\pi^0$	298 ± 25	23.2	5.96	5.35	8.22
$\bar{\Sigma}^-\pi^-\pi^+$	1066 ± 49	23.2	5.48	5.34	8.04
$\bar{p}\pi^-\pi^+$	590 ± 48	60.2	⋯	⋯	20.06

Table B6. ST yields, ST and DT efficiencies of various tag modes for the data sample at $\sqrt{s} = 4698.82\,\text{MeV}$. The uncertainties are statistical only. The quoted efficiencies do not include any subdecay BFs. Entries of "⋯" are for the cases where knowledge of the DT efficiencies are not required in the analysis.

Tag mode	$N_i^{\rm ST}$	$\varepsilon_i^{\rm ST}(\%)$	$\varepsilon_i^{\rm DT}(n\pi^+\pi^0)(\%)$	$\varepsilon_i^{\rm DT}(n\pi^+\pi^-\pi^+)(\%)$	$\varepsilon_i^{\rm DT}(nK^-\pi^+\pi^-)(\%)$
$\bar{p}K_S^0$	958 ± 33	47.5	12.29	11.25	17.86
$\bar{p}K^+\pi^-$	5167 ± 80	46.3	10.62	10.49	16.16
$\bar{p}K_S^0\pi^0$	471 ± 34	18.9	4.66	4.52	6.62
$\bar{p}K_S^0\pi^-\pi^+$	462 ± 31	19.5	4.21	4.11	6.33
$\bar{p}K^+\pi^-\pi^0$	1389 ± 74	17.5	⋯	4.02	6.63
$\bar{\Lambda}\pi^-$	538 ± 25	39.4	9.80	8.81	13.64
$\bar{\Lambda}\pi^-\pi^0$	1301 ± 49	17.9	3.93	3.73	5.82
$\bar{\Lambda}\pi^-\pi^+\pi^-$	639 ± 34	14.6	2.73	2.63	3.82
$\bar{\Sigma}^0\pi^-$	371 ± 22	24.3	6.12	5.75	8.4
$\bar{\Sigma}^-\pi^0$	251 ± 24	22.2	5.62	5.18	7.90
$\bar{\Sigma}^-\pi^-\pi^+$	956 ± 48	22.2	5.25	5.07	8.16
$\bar{p}\pi^-\pi^+$	459 ± 47	55.9	⋯	⋯	19.66

References

[1] L. L. Chau, H. Y. Cheng, and B. Tseng, Phys. Rev. D **54**, 2132 (1996)
[2] H. Y. Cheng, Chin. J. Phys. **78**, 324 (2022)
[3] C. D. Lü, W. Wang, and F. S. Yu, Phys. Rev. D **93**, 056008 (2016)
[4] C. Q. Geng, Y. K. Hsiao, C. W. Liu *et al.*, J. High Energy Phys. **11**, 147 (2017)
[5] C. Q. Geng, Y. K. Hsiao, C. W. Liu *et al.*, Eur. Phys. J. C **78**, 593 (2018)
[6] C. Q. Geng, Y. K. Hsiao, C. W. Liu *et al.*, Phys. Rev. D **97**, 073006 (2018)
[7] C. Q. Geng, Y. K. Hsiao, C. W. Liu *et al.*, Phys. Rev. D **99**, 073003 (2019)
[8] C. Q. Geng, C. W. Liu, T. H. Tsai *et al.*, Phys. Rev. D **99**, 114022 (2019)
[9] X. G. He, Y. J. Shi, and W. Wang, Eur. Phys. J. C **80**, 359 (2020)
[10] H. J. Zhao, Y. L. Wang, Y. K. Hsiao *et al.*, J. High Energy Phys. **02**, 165 (2020)
[11] H. B. Li and X. R. Lyu, Natl. Sci. Rev. **8**, nwab181 (2021)
[12] M. Ablikim *et al.* (BESIII Collaboration), Phys. Rev. Lett. **116**, 052001 (2016)

[13] M. Ablikim *et al*. (BESIII Collaboration), Phys. Rev. D **95**, 111102 (2017)
[14] M. Ablikim *et al*. (BESIII Collaboration), Phys. Rev. Lett. **118**, 112001 (2017)
[15] M. Ablikim *et al*. (BESIII Collaboration), Phys. Lett. B **783**, 200 (2018)
[16] M. Ablikim *et al*. (BESIII Collaboration), Chin. Phys. C **43**, 083002 (2019)
[17] M. Ablikim *et al*. (BESIII Collaboration), Phys. Rev. D **99**, 032010 (2019)
[18] M. Ablikim *et al*. (BESIII Collaboration), Phys. Rev. Lett. **128**, 142001 (2022)
[19] R. Aaij *et al*. (LHCb Collaboration), Phys. Rev. D **97**, 091101 (2018)
[20] S. X. Li *et al*. (Belle Collaboration), Phys. Rev. D **103**, 072004 (2021)
[21] S. X. Li *et al*. (Belle Collaboration), Phys. Rev. D **104**, 072008 (2021)
[22] M. Gronau and J. L. Rosner, Phys. Rev. D **97**, 116015 (2018)
[23] P. A. Zyla *et al*. (Particle Data Group), Prog. Theor. Exp. Phys. **2022**, 083C01 (2022)
[24] C. P. Jia, D. Wang, and F. S. Yu, Nucl. Phys. B **956**, 115048 (2020)
[25] M. Saur and F. S. Yu, Sci. Bull. **65**, 1428 (2020)
[26] K. K. Sharma and R. C. Verma, Phys. Rev. D **55**, 7067 (1997)
[27] J. Adler *et al*. (MARKIII Collaboration), Phys. Rev. Lett. **62**, 1821 (1989)
[28] M. Ablikim *et al*. (BESIII Collaboration), Chin. Phys. C **40**, 063001 (2016)
[29] M. Ablikim *et al*.(BESIII Collaboration), Chin. Phys. C **39**, 093001 (2015)
[30] M. Ablikim *et al*. (BESIII Collaboration), Chin. Phys. C **46**, 113003 (2022)
[31] M. Ablikim *et al*. (BESIII Collaboration), Chin. Phys. C **46**, 113002 (2022)
[32] M. Ablikim *et al*. (BESIII Collaboration), Nucl. Instrum. Meth. A **614**, 345 (2010)
[33] C. H. Yu *et al.*, Proceedings of IPAC2016, Busan, Korea, 2016
[34] M. Ablikim *et al*. (BESIII Collaboration), Chin. Phys. C **44**, 040001 (2020)
[35] X. Li *et al*., Radiat. Detect. Technol. Methods **1**, 13 (2017)
[36] Y. X. Guo *et al*., Radiat. Detect. Technol. Methods **1**, 15 (2017)
[37] P. Cao *et al*., Nucl. Instrum. Meth. A **953**, 163053 (2020)
[38] S. Jadach, B. F. L. Ward and Z. Was, Phys. Rev. D **63**, 113009 (2001)
[39] D. J. Lange, Nucl. Instrum. Meth. A **462**, 152 (2001)
[40] R. G. Ping, Chin. Phys. C **32**, 599 (2008)
[41] J. C. Chen, G. S. Huang, X. R. Qi, D. H. Zhang and Y. S. Zhu, Phys. Rev. D **62**, 034003 (2000)
[42] S. Agostinelli *et al*. (GEANT4 Collaboration), Nucl. Instrum. Meth. A **506**, 250 (2003)
[43] J. Allison *et al*., IEEE Trans. Nucl. Sci. **53**, 270 (2006)
[44] H. Albrecht *et al*. (ARGUS Collaboration), Phys. Lett. B **241**, 278 (1990)